Title

The environmental toxicant ziram enhances neurotransmitter release and increases neuronal excitability via the EAG family of potassium channels

Authors

Harrigan, Jenna
Brambila, Daisy F
Meera, Pratap
et al.

Publication Date

2020-09-01

DOI

10.1016/j.nbd.2020.104977

HHS Public Access

Author manuscript

Neurobiol Dis. Author manuscript; available in PMC 2021 October 09.

Published in final edited form as:

Neurobiol Dis. 2020 September ; 143: 104977. doi:10.1016/j.nbd.2020.104977.

The environmental toxicant ziram enhances neurotransmitter release and increases neuronal excitability via the EAG family of potassium channels

Jenna Harrigan[1], **Daisy F. Brambila**[2], **Pratap Meera**[2], **David E. Krantz**[1,3,4,*], **Felix E. Schweizer**[1,2,4,*]

[1]Molecular Toxicology PhD Program, School of Public Health, University of California Los Angeles

[2]Department of Neurobiology, David Geffen School of Medicine, University of California Los Angeles

[3]Department of Psychiatry and Biobehavioral Sciences, David Geffen School of Medicine, University of California Los Angeles

[4]Brain Research Institute, University of California Los Angeles

Abstract

Environmental toxicants have the potential to contribute to the pathophysiology of multiple complex diseases, but the underlying mechanisms remain obscure. One such toxicant is the widely used fungicide ziram, a dithiocarbamate known to have neurotoxic effects and to increase the risk of Parkinson's disease. We have used *Drosophila melanogaster* as an unbiased discovery tool to identify novel molecular pathways by which ziram may disrupt neuronal function. Consistent with previous results in mammalian cells, we find that ziram increases the probability of synaptic vesicle release by dysregulation of the ubiquitin signaling system. In addition, we find that ziram increases neuronal excitability. Using a combination of live imaging and electrophysiology, we find that ziram increases excitability in both aminergic and glutamatergic neurons. This increased excitability is phenocopied and occluded by null mutant animals of the *ether a-go-go* (*eag*) potassium channel. A pharmacological inhibitor of the temperature sensitive hERG (human *ether-a-go-go* related gene) phenocopies the excitability effects of ziram but only at elevated temperatures. *Seizure* (*sei*), a fly ortholog of hERG, is thus another candidate target of ziram. Taken together, the eag family of potassium channels emerges as a candidate for mediating some of the toxic effects of ziram. We propose that ziram may contribute to the risk of complex human diseases by blockade of human eag and sei orthologs, such as hERG.

[*]Corresponding authors. dkrantz@ucla.edu, felixs@ucla.edu.

Credit Author Statement

JH, DFB, DEK and FES conceptualized the work and wrote the manuscript. PM conducted the whole-cell recordings in the adult. JH conducted the calcium imaging experiments. JH and DFB conducted most of the experiments and composed the figures. JH, DFB and PM did the analysis of the data. FES wrote the custom software. All co-authors read and approved the final version of the paper. DEK provided funding for the majority of the experiments.

No financial conflicts of interest are noted.

Keywords

Ziram; pesticide; fungicide; neurotoxicant; synaptic transmission; synaptic vesicle; release probability; neuronal excitability; E1 ligase; potassium channel; ether-a-go-go; hERG; *sei* channel; complex diseases

Introduction

Environmental risk factors associated with an increased risk for complex human diseases include man-made toxicants such as pesticides (Parron et al., 2011; Mostafalou and Abdollahi, 2013; Stallones and Beseler, 2016). The mechanisms by which toxicants increase the risk for neurological disease include individual, well-characterized pathways such as the disruption of the mitochondrial respiratory chain and increased oxidative stress (Cannon and Greenamyre, 2011; Mostafalou and Abdollahi, 2013; Nandipati and Litvan, 2016). However, toxicants can also initiate neurological disease states via other, less well-characterized pathways (Heinemann et al., 2016; Chen et al., 2018; Muddapu et al., 2019). Individual toxicants also may have more than one target and disruption of multiple pathways by the same toxicant could be required to increase the risk for disease (Sulzer, 2007). Therefore, to understand the mechanisms by which environmental toxicants contribute to neurological disease states it will be necessary to discover the array of potential pathways by which they can disrupt neuronal activity.

Parkinson's disease (PD) is the second most common neurodegenerative disease and produces devastating changes in cognition, mood, gastrointestinal function and motor activity (de Lau and Breteler, 2006; Ascherio and Schwarzschild, 2016). Risk factors for PD include genetic mutations as well as environmental toxicants (Goldman, 2014). Genetic mutations account for rare variants that are inherited primarily in a Mendelian fashion (Lotharius and Brundin, 2002; de Lau and Breteler, 2006; Bezard et al., 2013). Similarly, rare forms of parkinsonism can be caused by toxicants such as MPTP (Parron et al., 2011; Duda et al., 2016; Langston, 2017). In contrast to these clearly defined environmental and genetic causes, most clinical PD cases are idiopathic and develop in response to a combination of multiple factors, similar to other "complex" diseases such as cardiovascular disease (Sulzer, 2007; Cosselman et al., 2015). Each risk factor may have a relatively small influence on the disease phenotype and, in isolation, cause only small changes in cell physiology or circuit activity, but act together to cause pathophysiological effects (Cannon and Greenamyre, 2011; Wang et al., 2011; Goldman et al., 2012; Ascherio and Schwarzschild, 2016).

Model systems provide useful platforms to assess the mechanisms by which toxicants may compromise neuronal function (Bezard et al., 2013). Long-term exposures are particularly important to determine whether a toxicant or combination of toxicants will lead to cell death and thus contribute to the clinical phase of neurodegenerative diseases (Cannon and Greenamyre, 2011; Parron et al., 2011; Ascherio and Schwarzschild, 2016). Long-term studies can reveal additional developmental and behavioral effects that precede or are distinct from later degenerative outcomes (Cao et al., 2019). Acute exposures on the other hand may be used to determine the more proximal targets of toxicants and the

mechanisms by which toxicants initiate the disruption of neuronal activity (Cannon and Greenamyre, 2011; Heinemann et al., 2016). Importantly, a relatively acute cellular phase may be distinguishable from a later, more chronic clinical phase in neurodegenerative disease processes (De Strooper and Karran, 2016; Noyce et al., 2016).

Ziram is a widely used fungicide linked to a 3-fold increased risk of developing PD in both agricultural employees as well as people living adjacent to agricultural fields and chronically exposed to high concentrations of pesticides (Wang et al., 2011). While several cellular effects and molecular targets have been proposed, the mechanisms by which ziram disrupts neuronal activity and thereby increases the risk of human diseases are not known (Chou et al., 2008; Fitzmaurice et al., 2014; Martin et al., 2016). To address this question, we have taken an open-ended approach to determine how ziram affects neuronal activity in the model system *Drosophila melanogaster*. We used *Drosophila* in part because of the extensively developed genetic toolset that allows the use of mutations to explore mechanistic pathways (Ganetzky and Wu, 1986; Hales et al., 2015). Using live imaging and electrophysiological assays we show that ziram can disrupt neuronal activity via at least two pathways: 1) An increase in vesicle release probability mediated through the initial steps within the ubiquitin signaling system and; 2) an increase in excitability mediated by inhibition of evolutionarily conserved member(s) of the eag family of potassium channels. We propose that ziram acts via these and perhaps other pathways to increase the risk of human neurological disease, especially during the early cellular phase of pathophysiology before overt neurodegeneration has begun (De Strooper and Karran, 2016; Noyce et al., 2016).

Materials & Methods

Drosophila Stocks and Husbandry

Flies were raised at 25°C under a 12 hour day/night cycle on a conventional cornmeal/molasses/yeast/agar medium. The GAL4-UAS system was employed for targeted expression of UAS-GCaMP6m (chromosome III insertion) in octopaminergic cells using Tdc2-GAL4 as described (Martin et al., 2016). eag^{sc29} is a null allele and eag^{1} is a hypomorphic allele of the *eag* potassium (K) channel (Xing and Wu, 2018). Additional K channel mutations used include $Shaker^{5}$ (Sh^{5}), a missense point mutation, and $Shaker^{KS133}$(Sh^{KS133}), a null allele of the *Shaker (Sh)* gene, and *slowpoke1 (*slo^{1}*),* a null allele of the *slowpoke* (*slo*) gene. All lines are available from the Bloomington Stock Center unless otherwise noted. w^{1118} was used as a control line for K channel mutants and for all other experiments.

Dissection of *Drosophila* Larvae and Adults

Third instar wandering larvae were dissected to expose the muscles in the body wall in calcium free HL3.1 solution (Feng et al., 2004; Imlach and McCabe, 2009). For neuromuscular junction (NMJ) recordings, two dissections were used to differentiate the contribution of ziram to central versus peripheral nerves. To ablate all contributions of neurons and processes within the ventral nerve cord (VNC), the central nervous system (CNS) was removed and all processes at the base of the VNC were severed leaving only the free hanging nerves containing motoneuron axons (Fig. 5A). In a second preparation, a cut was made across segment A2 of the larval VNC, leaving the abdominal segments

of the VNC intact and attached to the nerves that project to the body wall (Fig. 5B). For calcium imaging and electrophysiology of aminergic neurons in the adult abdominal ganglion, female flies aged 3 to 7 days post-eclosion were used. The flies were pinned on a Sylgard platform or glued with UV-cured glue (Bondic) onto a glass coverslip and the cuticle was removed to expose the abdominal ganglion. For the “ventral” preparations a small window of cuticle was removed on the ventral surface of the animal to expose the ventral surface of the abdominal ganglion, which lies just below the cuticle. For “dorsal” dissections, the dorsal surface of the cuticle was cut and pinned back, and the overlying flight muscle was removed to expose the dorsal surface of the abdominal ganglion. The axons at the base of the abdominal ganglion were severed in “dorsal cut” preparations and were left intact in the dorsal and ventral “intact” preparations (Fig. 2A, E).

Solutions

Ziram stock solution (10 mM in DMSO) was prepared weekly and frozen (−20 C) as aliquots. Working dilutions from the aliquoted stock were prepared daily. KCl (3M) was used to fill sharp electrodes for intracellular recordings and HL3.1 (pH = 7.3; 70 mM NaCl, 5 mM KCl, 5 mM trehalose, 2 mM $CaCl_2$, 4 mM $MgCl_2$, 115 mM sucrose, 10 mM $NaHCO_3$) was used as external solution for all NMJ experiments as described in Feng et al. (2004). The internal solution for whole-cell patch clamp contained 140 mM potassium aspartate, 10 mM HEPES, 1 mM KCl, 4 mM Mg-ATP, 0.5 mM Na_3GTP, 1 mM EGTA (pH 7.3) and external solution was HL3.1 (see above). Ziram was purchased from ChemService Inc. and G5 was purchased from Santa Cruz Biotechnology. PYR 41, lactacystin, and NSC 624206, and disulfiram were purchased from Tocris/R&D Systems. Tetrodotoxin (TTX) was purchased from Alomone labs. Additional reagents were purchased from Sigma unless stated otherwise.

Electrophysiology

For intracellular recordings in larval abdominal wall muscle, recording pipettes with a resistance of 20–35 MΩ were pulled on a Sutter P-97 puller from 0.5mm ID, 1.0mm OD borosilicate glass (with filament; Sutter) and filled with 3M KCl. For miniature end junction potential (mini) post synaptic recordings, the electrode was inserted into muscle 6 in abdominal segments A3 or A4. Control solution was perfused (1 ml/min) during a five-minute baseline and then switched to another control or a test solution for the remainder of the experiment. To generate experimentally evoked excitatory junctional potentials (evoked potentials) at the larval NMJ, the relevant segmental nerve was sucked into a fire polished suction electrode (5–15 μm inner diameter), filled with calcium free HL3.1 and stimulated every 30 seconds to evoke action potentials (APs). The 1 ms stimulation current was adjusted to 1.5 times the threshold current to ensure AP initiation (30 μA-1mA).

The membrane potential in larval muscle was recorded using an Axoclamp 2B or a Multiclamp 700A (Molecular Devices) amplifier, amplified (100x) and low-pass filtered (Axoclamp: 3 kHz, Brownlees Instruments; Multiclamp: 4kHz). Data were digitized at 20 kHz using a National Instruments data acquisition board and software custom written in LabView (National Instruments, Inc). Recordings were analyzed offline using an event detection algorithm based on threshold crossings of the first derivative (LabView).

Data normalization, graphing and further analysis were done using Origin (OriginLab Corporation).

For experiments conducted at elevated temperatures, a Warner SB TC-324B single channel temperature controller was used to elevate and maintain the perfusion solution temperature surrounding the larval preparation to 40°C. In addition, a Styrofoam enclosure was constructed around the recording microscope and a mini-space heater was used to elevate the ambient temperature within the enclosure to 32–38°C.

For electrophysiological recordings in the abdominal ganglion of adult female flies, Tdc2-positive octopaminergic neurons were recorded from a whole-cell patch clamp configuration. 1.5mm OD, 0.86mm ID Borosilicate glass electrodes (7–9 MΩ) were filled with the whole-cell patch clamp internal solution (see solutions above). The preparation was perfused with HL3.1 solution and continuously aerated with carbogen (95% O_2/5% CO_2). 3% Protease IV was puffed onto the preparation for 3–10 minutes prior to recording to remove the glial sheath that surrounds the ganglion (Ryglewski and Duch, 2012). Recordings were made using the current clamp mode of the whole-cell patch clamp technique. To measure AP threshold and AP number, a current was injected that ramped linearly over one second from a starting level of −50 pA to a maximal level of 0 pA. In the next trial the starting current was still −50 pA but ramped to a maximal current of +50 pA, then in the next trail to +100 pA, until a maximal current of +450 pA was reached. The number of APs for each ramp was divided by the number of APs obtained at +450 pA in the control condition to obtain the normalized values shown in Fig 3C. Recordings were made using a MultiClamp 700B Amplifier, filtered at 4 kHz, and sampled at 10 kHz with a Digidata 1300b under control of pClamp (Molecular Devices).

Calcium Imaging

To visualize intracellular calcium levels, UAS-GCaMP6m was expressed in octopaminergic cells using Tdc2-GAL4 (Cole et al., 2005; Chen et al., 2013). Third instar larval preparations were dissected as described previously in calcium free HL3.1 solution (see Solutions) and then washed 3x with chilled HL3.1 solution containing 2 mM Ca^{2+} prior to imaging (Martin et al., 2016). Control solution or a test drug was added via perfusion to the bath after a 1–2 minute baseline recording at ambient temperature. Nerve terminals and cells were imaged using a Zeiss Axio Examiner Z1 microscope and Zeiss Achroplan water immersion objective (40x, 1.0 N.A.) with a CCD camera (Andor iXon 897, Oxford Instruments, Oxfordshire, England) and a capture rate of 11.9 frames/s using Andor IQ2 software. A DG4 light source (Sutter, Novato, CA) with a GFP Brightline® Filter Set (Semrock, Rochester, NY) was used for illumination. Segment A4 of muscle 13 was visualized for all experiments as previously described (Martin et al., 2016). For analysis of the GCaMP experiments, 3–5 individual boutons were selected per axon branch using ImageJ (NIH) and the Time Series Analyzer plugin. The individual boutons were background subtracted and then averaged per frame. ΔF/F was quantified as ΔF/F= [(F peak - F baseline)/ F baseline] as reported in Martin et al. (2016).

Experimental Design and Statistical Analysis

For each calcium imaging recording, 3–5 regions of interest from one preparation were imaged within a single 40x field of view and averaged to obtain a single observation with an n of 4–15 animals used for statistical analysis. For electrophysiology experiments, normalized frequency and amplitudes of minis and end junction potentials (EJP) were divided by their respective five-minute baseline interval before drug was added. The normalized and raw frequency and amplitudes were plotted over time or represented as scatterplots with mean ± SEM and used to quantify the effect of each mutant line and drug concentration. An effect was judged as statistically significant if $p<0.05$ in an ANOVA with a post-hoc Dunn-Sidak test for multiple comparisons, a Wilcoxon signed rank test, or a t-test when applicable. The analysis of the data in Figure 5K was made based on comparing means and differences in means using the bootstrap method implemented in Labview (Efron and Tibshirani, 1991; Efron and Hastie, 2016)

Results

Ziram dose-dependently increases excitability of octopaminergic neurons

We previously reported that a high concentration of ziram (20 μM) causes synchronized calcium events at octopaminergic processes and nerve terminals at the larval NMJ (Martin et al., 2016). Here, we expanded our dose response curve to include concentrations previously used to test the toxicity of ziram (1–20 μM; Fig. 1 A–D) (Chou et al., 2008; Rinetti and Schweizer, 2010; Dennis and Valentine, 2015). Although concentrations as low as 1 μM induce synchronized calcium events in octopaminergic processes, higher concentrations generated more frequent events (Fig. 1B, D) and required a shorter incubation prior to the initiation of events (Fig. 1C). The time-period to the first calcium event differed between high (20 and 10 μM) versus low concentrations (1 and 2 μM) of ziram (Two-way ANOVA and post-hoc Dunn-Sidak: n=3–12, $p< 0.001$ per concentration). We also found that the *frequency* of calcium events at 25–30 minutes post-ziram addition was increased at higher concentrations, with 20 μM ziram significantly different from both 1 and 2 μM (One-way ANOVA and post-hoc Dunn-Sidak: n=4–14, $p=0.004$ and $p<0.001$, respectively).

To determine whether the effects of ziram would generalize to octopaminergic cells beyond those innervating the larval NMJ, we tested ziram at a well-defined cluster of midline neurons in the adult abdominal ganglion (Fig. 2A, E) (Rodriguez-Valentin et al., 2006; Rezaval et al., 2012). Application of 20 μM ziram either induced calcium events in octopaminergic cell bodies and processes within the ganglion in preparations with no baseline calcium activity or increased the frequency in preparations with spontaneous activity at baseline (Fig. 2C, F). Approximately half of these preparations showed spontaneous activity at baseline.

To help define ziram's site of action, we severed the nerves containing the distal axons and terminals of the octopaminergic neurons ("dorsal cut" dissection, see Fig. 2A). These preparations showed no spontaneous activity at baseline, and in contrast to dorsal "intact" preparations, ziram failed to increase calcium events in the cell bodies (Fig. 2A, D). This

suggests that ziram's major site of action may be localized to or depend on factors in distal axonal processes or nerve terminals rather than somatodendritic sites (Fig. 2D).

Octopaminergic cell bodies within the abdominal ganglia localize to the ventral surface and are difficult to detect when visualized in dorsal preparations ("dorsal", see Fig. 2A). To better visualize individual cells and distinguish fluorescence in somata versus their adjacent processes, we inverted our preparation so that the ventral surface of the ganglion was facing the objective ("ventral", see Fig. 2E). Application of ziram increased the frequency of calcium signals in most if not all the visualized cells (Fig. 2E, F). Interestingly, calcium signals in individual octopaminergic neurons were not synchronized (Fig. 2E, F), suggesting heterogeneous excitability within the cluster of neurons.

To more directly test whether ziram increases electrophysiological excitability, we recorded from octopaminergic neurons in the abdominal ganglion of adult flies using whole-cell patch clamp. Increased excitability could manifest as a membrane potential depolarization, a decrease in the amount of current required to bring the neuron to threshold irrespective of membrane potential, or a combination of both mechanisms. Consistent with the first mechanism, perfusion of 10 μM ziram during a whole-cell current clamp recording depolarized the resting membrane potential by 8.2 ± 2.4 mV relative to controls (Fig. 3A; n=5, p=0.027; two-way t-test), thus bringing them closer to firing threshold. To test whether the amount of current required to elicit an AP might also be decreased, we used current ramp injections to measure threshold and AP number (see Methods). After application of ziram, less current was required to trigger an AP, consistent with a decreased AP threshold (Fig. 3B, C). To disambiguate depolarization and AP threshold, we kept the membrane potential hyperpolarized to −63 ± 1 mV by injecting bias current (Fig, 3B, C; black and red trace/curves). Ziram still decreased the minimum amount of current required to elicit an AP compared to controls and increased the mean number of APs at each current ramp injection (Fig 3B, C; black and red traces/curves). For example, the average number of APs elicited during a −50 pA to 300 pA ramp injection increased from 4.8 to 8 at −63 mV and from 6.8 to 13.4 at the cell's resting potential (Wilcoxon nonparametric test, p=0.03 both at the cell's resting potential and at −63mV; Fig. 3B, C). Together these data demonstrate that ziram increases the excitability of octopaminergic neurons both by depolarizing the membrane potential and by lowering the threshold for AP firing.

Ziram increases the excitability of glutamatergic neurons

Using calcium imaging, we previously did not detect an increase in excitability in glutamatergic neurons innervating the larval NMJ (Martin et al., 2016). However, recent data show that calcium homeostasis differs between octopaminergic and glutaminergic neurons at the NMJ (Xing and Wu, 2018). Octopaminergic neurons show detectable calcium signals in response to a wide range of stimulation frequencies, but glutamatergic neurons, while responsive to stimulation, show a similarly robust calcium response only following high frequency stimulation and pharmacological inhibition of channel activity (Xing and Wu, 2018). We therefore reasoned that ziram might indeed stimulate *action potentials* in both glutamatergic and octopaminergic cells but fail to generate a *detectable calcium signal* in glutamatergic processes. To test this hypothesis, we performed sharp electrode

electrophysiological recordings from muscle 6 at the larval NMJ (without VNC) (Imlach and McCabe, 2009).

Glutamatergic motoneuron APs elicit the exocytotic release of glutamate from *multiple* vesicles, triggering a large, ionotropic postsynaptic response, which can be measured in the postsynaptic muscle in the larval body wall as an excitatory end junction potential (EJP) of several millivolts in amplitude. These large EJPs, which occur in response to a presynaptic AP are easily distinguishable from the small, miniature end junction potentials (minis), which have an amplitude of ≤1 mV and occur in response to transmitter released from a *single* vesicle. We can thus take the presence of these larger amplitude EJPs at the larval NMJ as an indicator of presynaptic APs, a proxy of increased neuronal excitability. If ziram increases the excitability of glutamatergic neurons to the point of AP firing, we expect to detect 'spontaneous' EJPs of several millivolts in amplitude. Indeed, when we measured the muscle membrane potential at the NMJ intracellularly, we observed 'spontaneous' EJPs following application of ziram in preparations without the VNC (Fig. 4A, B). Ziram-induced EJP events were sensitive to the sodium channel blocker tetrodotoxin (TTX; Fig. 4B, C). Since contraction-initiating APs in the muscles of the NMJ depend on calcium channels rather than on TTX-sensitive sodium channels (Littleton and Ganetzky, 2000), we conclude that the large ziram-induced EJPs are triggered by presynaptic APs.

To further explore the electrophysiological response to ziram, we applied ziram at increasing concentrations and quantified the time to first EJP (Fig. 4D). In contrast to the modest but significant effects of ≤1 μM ziram on octopaminergic cells, we did not detect any EJPs in larval muscle at this low concentration in preparations without a VNC (Fig. 4D). Our data suggest that ziram may directly increase the excitability of both octopaminergic and glutamatergic neurons and that octopaminergic neurons may be more sensitive to the effects of ziram. However, previous reports show that octopamine can modulate glutamate release from glutamatergic (Type I) terminals and thus affect electrophysiological responses measured at the NMJ (Kutsukake et al., 2000; Nagaya et al., 2002). While muscle 6 is not a target for major octopaminergic innervation (Atwood et al., 1993; Monastirioti et al., 1995), we cannot rule out the possibility that the electrophysiological responses we observed were caused by the activation of octopaminergic (Type II) terminals by ziram, and the subsequent, indirect stimulation of Type I terminals by octopamine. Although we find that ziram concentrations as low as 1 μM can induce synchronized calcium events in octopaminergic processes, higher concentrations and more frequent events (Fig. 1B, D) might be required to release enough octopamine to stimulate Type I terminals.

Differential effects of ziram across different sites of action

In addition to acting peripherally on Type I terminals (Kutsukake et al., 2000; Nagaya et al., 2002) octopamine can also act centrally on glutamatergic motoneurons to regulate their electrical activity and locomotor output (Saraswati et al., 2004; Fox et al., 2006; Simon et al., 2009; Koon and Budnik, 2012; Selcho et al., 2014). This suggests that ziram could have non-linear effects not only at the periphery but also centrally. To explore this idea, we compared the effects of ziram in two types of preparations in which the VNC was either completely severed from the peripheral nerves or a portion of the VNC was left

intact and attached to the peripheral nerves. For the intact VNC preparation, the descending inputs from the CNS to the VNC were severed to avoid contractions driven by CNS input. Consistent with previous reports that central octopaminergic cells can modulate motoneuron activity (Fox et al., 2006; Simon et al., 2009), we observe an increase in EJP frequency with octopamine bath application to preparations with the distal VNC left attached (data not shown). Similarly, we observe an increase in the fraction of experiments with detectable EJPs at 1 μM ziram and an increase in EJP frequency in preparations with the VNC attached (Fig. 5F, K). By contrast, when connections of the VNC to the body wall were severed, leaving only the free-hanging nerves (Fig. 5A), 1 μM ziram had no effect (Fig. 5E, K). Application of ziram at concentrations above 1 μM elicited EJPs in both preparations, but the frequency was higher in preparations with the VNC intact (Fig. 5K; 1μM n = 6 & 12, $p < 0.03$; 2μM: n=8 & 13, $p < 0.01$; 10 μM: n=9 & 14, $p < 0.001$ (see methods)). These data are consistent with the idea that depending on the site of action, the effects of ziram on excitability can differ. The similarity between the effect of ziram at 1 μM and the effect of octopamine in VNC-attached preparations suggest that the central site of action of 1 μM ziram could be octopaminergic processes that regulate motoneuron excitability; however, other pathways within the VNC that regulate motoneuron activity also represent potential targets.

Ziram increases the probability of synaptic vesicle release

During our recordings of spontaneous EJPs we observed an increase in the frequency of mini events; however, this effect was partially obscured by ziram-induced spontaneous EJPs (Fig. 4B). Thus, we applied TTX to block the presynaptic APs required for EJPs to allow for the analysis of minis (Fig. 4C). We indeed observed a clear, ziram-induced increase in the frequency but not the amplitude of spontaneous minis, suggesting an increase in presynaptic vesicle release probability (Fig. 6A–C). The ziram-induced increase in mini frequency appeared to be independent of extracellular calcium concentration and occurred in HL3.1 solution containing calcium concentrations as low as 0.2 mM (n= 8; Fig. 6B).

Higher doses of ziram (10 μM and 20 μM) led to an increase in mini frequency (Fig. 6B), followed by a strong depolarization of the membrane potential (data not shown; see Fig. 3A for comparison). The concomitant decrease in driving force for currents through the glutamate receptors led to a decrease in mini amplitude, which made it progressively difficult to resolve low amplitude minis from noise. While this hindered the establishment of a rigorous dose-response relationship, higher doses elicited increases in frequency earlier during the experiment (Fig. 6B).

An increase in mini frequency is usually interpreted as an increase in the probability of the *spontaneous* release of individual synaptic vesicles. An increase in vesicle release probability might further reveal itself through an increased amplitude of the postsynaptic response to an experimentally triggered AP. These investigator-induced post synaptic events will be termed “evoked potentials” to differentiate them from the EJPs resulting from the spontaneous APs induced by ziram (see Fig. 4B). Thus, to determine whether ziram increases the probability of synchronous vesicle release, we measured the amplitude of evoked potentials following perfusion with ziram (Fig. 6D, F, G). We observe a consistent

increase in the amplitude of evoked potentials, which peaked after 10 minutes in ziram and then declined (Fig. 6F). Quantification of evoked potential amplitudes at 10 minutes showed an increase as high as 3-fold in the presence of ziram relative to controls (Fig. 6D, F). These data are consistent with ziram increasing the probability of both spontaneous and synchronous evoked vesicle release.

We noted that the dose of ziram required to increase excitability was higher than the dose required to increase the probability of release. At a low dose of ziram (1 μM) both the evoked potential amplitude and mini frequency increased (Fig. 6B, G), however there was no detectable effect on the excitability of glutamatergic neurons at this dose (see Figs. 4D, 5E). These differences suggest that the mechanisms by which ziram increases the probability of vesicle release might be distinct from those responsible for increased excitability. To investigate the pathways that lead to these two distinct neuronal effects, we tested compounds that share structural or toxicological properties with ziram.

Other PD-associated pesticides, dithiocarbamates, and zinc do not mimic either of the neuronal effects caused by ziram at the NMJ

Ziram is composed of two identical, anionic dithiocarbamate molecules bound by a positively charged zinc atom raising the possibility that zinc alone might contribute to the effects of ziram (Fig. 7A). We tested zinc chloride at the NMJ and did not observe an increase in release probability or excitability at concentrations as high as 10 μM (Fig. 7B).

To determine whether dithiocarbamates as a class might increase excitability or release probability, we tested the effects of two structurally related chemicals, maneb, a PD associated fungicide (Wang et al., 2011), and disulfiram, an aldehyde dehydrogenase inhibitor used to treat alcoholism (Fig. 7A, B) (Fitzmaurice et al., 2014). We found that disulfuram, but not maneb, increased the probability of release (Fig. 7B; disulfiram: Dunn-Sidak p=<0.001; maneb: Dunn-Sidak p=0.15) and neither maneb nor disulfuram induced EJPs (data not shown). These data indicate that although features common to dithiocarbamates such as free cysteines may contribute to changes in release probability or excitability, neither effect is common to all dithiocarbamates. In addition, the differential effects of disulfuram on excitability and release probability support the hypothesis that ziram could act through two distinct pathways.

Exposure to two other pesticides, paraquat and rotenone (Fig. 7A), has been strongly associated with an increased risk of developing PD (McCormack et al., 2002; Wang et al., 2011; Cao et al., 2018). However, neither toxin increased the frequency of minis (Fig. 7B) nor triggered EJPs, indicating that the neuronal effects of ziram are not shared by all toxicants associated with PD.

Disruption of the ubiquitin signaling system enhances vesicle release probability

Ziram was previously reported to increase mini frequency in mammalian cell cultures via inhibition of E1 ligase, the first element of the ubiquitin signaling system (Rinetti & Schweizer, 2010; Fig. 8A). We therefore examined whether pharmacologic inhibition of E1 ligase would similarly increase mini frequency at the *Drosophila* NMJ, and whether this intervention would also increase excitability. Consistent with the results in mammals,

we find that the E1 ligase inhibitors NSC and PYR41 increase mini frequency (Fig. 7B; one-way ANOVA and *post-hoc* Dunn-Sidak, PYR41: $p<0.001$; NSC: $p=0.012$). Consistent with an increase in release probability, PYR41 also increases evoked potential amplitude (one-way ANOVA and *post-hoc* Dunn-Sidak: $p=0.002$; Fig. 8D). Neither the proteasome inhibitor MG132 nor the deubiquitination inhibitor G5 showed a significant increase in mini frequency or evoked potential amplitude (Fig. 8B, D). Our results are in general agreement with previous work supporting the importance of the ubiquitin signaling system for synaptic transmission (DiAntonio and Hicke, 2004; Yi and Ehlers, 2005) and expand on those findings by suggesting that protein ubiquitination, rather than protein degradation, is crucial for the control of exocytosis.

We never observed spontaneous EJPs following perfusion with NSC, PYR41, MG132 or G5. This suggests that, unlike changes in the probability of release, the increase in excitability caused by ziram is not mediated via the ubiquitin signaling system (Fig. 8C). These results support the notion that the increase in excitability and vesicle fusion probability results from distinct molecular mechanisms.

eag potassium channel mutants phenocopy and occlude ziram-induced excitability

We next explored mechanisms of ziram-induced excitability. Since K channels are critical regulators of neuronal excitability, we tested whether the broad-spectrum K channel blocker, tetraethylammonium (TEA), would replicate the effect of ziram on excitability. Indeed, TEA phenocopied ziram at octopaminergic terminals and induced spontaneous calcium signals (data not shown). We therefore hypothesized that ziram inhibits one or more K channels (Shieh et al., 2000; Bauer and Schwarz, 2018). In order to determine whether inhibition of K channels contribute to ziram-induced excitability, we tested for the presence of EJP activity in *eag*, *Shaker* and *slowpoke* K channel mutant animals (Pallanck and Ganetzky, 1994; Jan and Jan, 2012).

Consistent with previous reports that spontaneous EJPs occur at baseline in animals with a null mutation in the *ether-a-go-go* (*eag*) K channel (Ganetzky and Wu, 1983; Ganetzky et al., 1999; Frolov et al., 2012), we observed EJPs at baseline in *eag*, but not in *Shaker* nor *slowpoke* mutants (Fig. 9A–D). In both eag^{1} and eag^{sc29} mutants, we observed EJPs with amplitudes ranging from 9–25 mV and frequencies ranging from 1–10 Hz, both of which remained constant throughout the experiment (Fig. 9A, B). We next performed occlusion experiments similar to classical epistasis studies to determine whether mutations in *eag* might affect pathways similar to or divergent from ziram (Mackay, 2015). Addition of 10 μM ziram to larvae homozygous for either a hypomorphic or null allele of *eag* did not detectably increase (or decrease) the frequency of spontaneous EJPs over a 30–60 minute period (Figs. 9A–B, 11C). *eag* mutant animals thus both mimic and occlude the effects of ziram. These results suggest that eag channel blockade may be the primary mechanism of ziram's effect on excitability.

In contrast to *eag*, application of ziram to *Shaker* and *slowpoke* elicited EJPs (Fig. 9C, D). These data indicate that the target of ziram is still available for blockade in these mutants and supports the involvement of eag-type channels, but not other K channels, in the ziram-induced excitability increase. In addition, we note that in *Shaker* mutants, some

of the EJPs occurring in response to ziram were slow depolarizing events, similar to those reported in *shaker* and *eag* double mutants (data not shown) (Ganetzky and Wu, 1983). We also observed slower repolarization of EJPs in the *slowpoke* mutants (Fig. 9D). These observations suggest that acute pharmacological block of eag channels by ziram acts akin to an *eag* null mutant in *modifying* the phenotype of *Shaker* and *slowpoke* mutants. In sum, our results support the hypothesis that increased neuronal excitability induced by ziram is likely due to disruption of a pathway involving eag or via direct inhibition of the eag channel.

eag mutations do not occlude ziram-induced mini frequency

To test the hypothesis that the mechanisms mediating ziram's effect on excitability and release probability are distinct, we examined the mini frequency of *eag*, *Shaker* and *slowpoke* mutant animals at baseline and following exposure to ziram (Fig. 9E, F). To allow for the quantification of minis in *eag* mutants, recordings were conducted in 1 μM TTX in order to block spontaneous EJPs. We did not observe a statistically significant difference in baseline mini frequency between wildtype and any of the K channel mutants (Fig. 9E). Application of 10 μM ziram elicited an increase in mini frequency in all K mutant lines tested, similar to the increase observed in wildtype animals (Fig. 9F). Two-way t-tests of each mutant showed that *eag*, *Shaker*, and *slowpoke* mutants have significantly increased mini frequencies in ziram relative to baseline (two-way t-tests: eag^{sc29} p=0.005; eag^{1} p= 0.03; Sh^{5} p=0.014; Sh^{KS133} p=0.03 (data not shown); $slowpoke^{1}$ p= 0.002; Fig 9F). Although the change in mini frequency in response to ziram appears less in *slowpoke* and *Shaker* animals than in *eag,* this difference in effect size was not significant. These results support the hypothesis that inhibition of eag contributes to increased excitability but not to increased vesicle release.

The hERG inhibitor E4031 increases the excitability effect of ziram at elevated temperatures

Drosophila express three members of the eag-type family of K channels*: eag*, eag-like (*elk*), and an eag-related (*erg*) K channel called seizure (*sei*) (Titus et al., 1997). elk remains poorly characterized, especially in *Drosophila*, but the sei channel, an ortholog of the hERG channel in humans, was intriguing because it was previously shown to regulate synaptic function and excitability at the NMJ (Lee and Wu, 2010; Frolov et al., 2012; Hill et al., 2019). However, unlike eag, which maintains baseline excitability, the sei channel has been proposed to regulate neuronal excitability in response to heat stress (Jackson et al., 1984; Titus et al., 1997; Hill et al., 2019). At elevated temperatures s*ei* mutant larvae showed a decreased time to paralysis (Zheng et al., 2014), seizures (Hill et al., 2019) and increased branching at the NMJ (Lee and Wu, 2010). In the heart, sei seems to be active at room temperature and play a role similar to hERG (Ocorr et al., 2017). To determine whether we could detect the activity of sei in our preparation, we used the hERG channel inhibitor E4031, which phenocopies cardiac arrythmias (Ocorr et al., 2017) and the heat sensitivity phenotype (Zheng et al., 2014) of *sei* mutant flies. E4031 (100 μM) had no effect on neuronal excitability (n=6, see Fig 11B) at room temperature, consistent with the idea that although sei may be active in the heart at room temperature, it may be much less active at lower temperatures in neurons (Jackson et al., 1984; Titus et al., 1997; Hill et al., 2019) similar to hERG (Vandenberg et al., 2006; Vandenberg et al., 2012). Intriguingly, at

elevated temperatures (40°C), E4031 elicited robust, spontaneous EJPs (Figs. 10A, 11B-C; Dunn-Sidak 40°C: 4.5±1.2, p= 0.006; 25°C: p= 0.07), consistent with E4031 inhibition of sei or another channel that only manifests itself at elevated temperatures. Alternatively, based on these data alone we could not exclude the possibility E4031 only blocked eag channels but in a temperature dependent fashion. If so, E4031 should show little or no activity in an *eag* null mutant animal.

To begin to explore the relationship between E4031, ziram and the eag mutant, we first performed control experiments to test whether temperature alone would have any effects on excitability. We again elevated the temperature of the preparations to 40°C, and quantified EJP frequency in either wildtype animals or *eag* mutants in the absence of either ziram or E4031. We did not observe EJPs in wildtype flies at 40°C (Figs. 10A, 11B–C) and indeed observed a counterintuitive, two-fold *decrease* in EJP frequency at 40°C in *eag* mutants (*eag* 25°C: 1.0±0.34 Hz; *eag* 40°C: 0.47±0.06 Hz; p= 0.004; Figs. 10B, 11B–C). This decreased EJP frequency became more pronounced over time at 40°C and might reflect an adaptive engagement of sei or other temperature sensitive channels to counteract hyperexcitability.

To test whether ziram could inhibit other eag family members such as sei in addition to eag channels, we next recorded from wildtype and *eag* null mutants at elevated temperatures (40°C) in the presence of ziram. Application of ziram to wildtype animals at 40°C led to a larger increase in EJP frequency compared to room temperature (w^{1118} 25°C: 2.0±1.2 Hz; w^{1118} 40°C: 10.4±2.1 Hz; Dunn-Sidak: p=.001; Figs. 10A, 11B). The increased EJP frequency at elevated temperatures could be due to contributions from both eag and other temperature sensitive channels. We therefore recorded from *eag* null mutants at elevated temperatures. Ziram enhanced the EJP frequency in *eag* mutants relative to control solution at 40°C (control 40°C: 0.47±0.06 Hz; ziram 40°C: 7.9±1.76 Hz; n=12, Dunn-Sidak: p=0.003; Figs. 10B, 11C) but not at room temperature (Figs. 9A, 9B, 11C). These data indicate that at 40°C, ziram can increase excitability via blockade of a molecular target distinct from eag. Importantly, since eag^{sc29} is a null allele, the increase in excitability is not due to further inhibition of eag.

To more specifically test whether the enhanced excitability effect of ziram at 40°C could be due to blockade of an E4031-sensitive channel such as sei, we applied E4031 to *eag* mutants at 25°C and 40°C. At 25°C, E4031 did not affect the EJP frequency in either w^{1118} or *eag* mutants (Fig. 11B, C). In contrast, E4031 did increase the EJP frequency in w^{1118} and *eag* mutants relative to control solution at 40°C (E4031 40°C: 7.13± 1.4 Hz; control 40°C: 0.47±0.06 Hz; Dunn-Sidak, p= 0.04; Figs. 10B, 11C). Our results are consistent with the idea that ziram inhibits both eag as well as a temperature and E4031 sensitive channel such as the sei ortholog hERG (Fig. 11A).

Discussion

A combination of genetic susceptibilities and environmental factors are thought to contribute to complex diseases such as cardiovascular disease and neurological conditions such as idiopathic PD and Alzheimer's disease (AD) (Szot, 2012; Baltazar et al., 2014; Yegambaram et al., 2015). While chronic exposure paradigms using a combination of chemicals will

be essential to determine how toxicants cause cell death in neurodegenerative diseases, acute exposure will pinpoint the initial targets of each toxicant that might be compromised long before the manifestation of clinical symptoms (Carvey et al., 2006; Heinemann et al., 2016). Ziram inhibits several biochemical pathways *in vitro* and *in vivo* (ALDH, E1 ligase, sodium-calcium exchanger, mitochondrial functions) but the relationship between these and other putative targets and human disease remains unclear (Rinetti and Schweizer, 2010; Fitzmaurice et al., 2014; Jin et al., 2014; Matei and Trombetta, 2016). We have used an open-ended approach in *Drosophila melanogaster* to investigate how ziram changes neuronal activity and identified a novel molecular pathway through which ziram can increase neuronal excitability.

Inhibition of E1 ligase increases synaptic vesicle release in cultured mammalian neurons, however the mechanisms remain unclear (Rinetti and Schweizer, 2010). Protein degradation via the proteasome is one possible pathway and has been suggested to regulate both the fly NMJ and mammalian synaptic activity (Speese et al., 2003; Rinetti and Schweizer, 2010; Ramachandran and Margolis, 2017; Ramachandran et al., 2018). However, the effects of proteasome inhibitors in our experiments differ from the effects of E1 ligase inhibitors. Ubiquitination can alter protein function in several ways that are distinct from proteasome dependent degradation, including the regulation of mitochondrial function, membrane trafficking, and endocytosis (DiAntonio and Hicke, 2004). Using ziram and other toxicants in combination with *Drosophila* genetics may help uncover the relevance of these non-degradative ubiquitin signaling system pathways to synaptic function and the early stages of complex diseases.

We previously reported that ziram causes an increase in the excitability of octopaminergic processes at the fly NMJ as observed through an increase in spontaneous calcium signals (Martin et al., 2016). However, an increase in calcium signals in presynaptic glutamatergic processes was not detected, possibly due to differences in calcium homeostasis between octopaminergic and glutamatergic axons (Xing and Wu, 2018). It thus seemed possible that ziram could elicit spontaneous APs in glutamatergic processes without causing detectable calcium transients. Hence, we re-examined the effects of ziram in glutamatergic neurons using electrophysiological methods. Indeed, ziram induces EJPs, suggesting that excitability of not only aminergic but also glutamatergic neurons is increased. We cannot rule out the possibility that ziram acts on octopaminergic neurons and that the release of octopamine, or indeed another transmitter, affects the changes in the glutamatergic neurons (Nagaya et al., 2002)

In addition to peripheral octopaminergic neuronal processes (Fig. 1A–D), we show that ziram increases the excitability of octopaminergic neurons in the adult CNS through a decrease in AP threshold and an increase in resting membrane potential (Fig. 3A–C). In the larval CNS, octopaminergic neurons regulate the activity of glutamatergic motoneurons that project peripherally to the NMJ (Simon et al., 2009; Selcho et al., 2014). Taking advantage of this locomotion circuit, we show that 1 μM ziram only elicits motoneuron APs if the distal portion of the VNC is left intact, but not when the VNC is completely severed and only the peripheral axons are present (Fig. 5B, F). This central interaction could be elicited through octopaminergic neurons, but additional pathways that regulate motoneuron output

might contribute to the increased excitability as well. These data support the idea that ziram may differentially affect some neuronal processes within a circuit, and that the effects of ziram on excitability can influence downstream outputs.

Ziram-induced increases in excitability of glutamatergic and octopaminergic neurons could propagate through circuits and thus indirectly affect other classes of neurons in the CNS in flies and perhaps mammals. We note that changes in the excitability of glutamatergic processes have been suggested to contribute to the pathophysiology of PD and the death of norepinephrine (NE) and dopaminergic (DA) neurons (Calabresi et al., 1993; Ridding et al., 1995; Ambrosi et al., 2014).

Potassium channels are exquisite regulators of neuronal activity that have been implicated in both the neuroprotective and pathophysiological effects of neurodegenerative diseases including both AD and PD (Dragicevic et al., 2015; Duda et al., 2016; Chen et al., 2018; Zott et al., 2018). For example, inactivation of K-ATP channels as well as inhibition of SK channels have been shown to block DA cell activity and cell death in rodent models (Liss et al., 2005; Duda et al., 2016). Similarly, overexpression of mutant alpha-synuclein increases DA neuron firing frequency by inhibiting A-type K channels (Subramaniam et al., 2014). In animal models of AD, ablation of the AD-linked β-secretase BACE1 reduces the amount of the m-current mediating Kv7.2/KCNQ2 (Lehnert et al., 2016) and decreased surface expression of the A-type K channel Kv3.4, both leading to enhanced excitability (Hartmann et al., 2018). Here we report that ziram acutely alters neuronal excitability by inhibiting members of the *ether-a-go-go* channel family, eag itself and possibly sei. A third member of this family, *elk*, remains poorly characterized in flies, and mutants do not show any apparent phenotype (Ganetzky et al., 1999). E4031 has been shown to inhibit hERG channels, but its actions on sei channels are not well characterized and are mostly inferred by E4031 mimicking and interacting with behavior observed in *sei* mutants (Zheng et al., 2014; Ocorr et al., 2017). Thus, while the sequence similarity between hERG and *sei* and the temperature dependent action of E4031 (Zheng et al., 2014; Ocorr et al., 2017) support the notion that E4031 blocks sei, additional channels could also serve as targets of ziram, and more direct experiments using sei mutants will be necessary to distinguish between these possibilities. It is also conceivable that ziram may act via a common upstream regulatory pathway rather than direct inhibition of K channels in the eag family and experiments using heterologously expressed cDNAs representing each channel will be necessary to address this question.

Eag and *sei* were discovered in *Drosophila* as hyperexcitability mutants at baseline and under heat stress, respectively, and *eag* led to the discovery of the eag family of channels in mammals (Ganetzky and Wu, 1983, 1986). Later the fly *seizure* locus was shown to encode the *Drosophila* homolog of hERG (Wang et al., 1997). Humans express eight orthologs of eag, originally classified as the KCNH family of K channels, which are grouped into the Kv10 (hEAG), Kv11 (hERG) and Kv12 (ELK) channels (Ganetzky et al., 1999). eag channels were previously reported to preferentially localize to neuronal axons and terminals rather than the somatodendritic compartment (Sun et al., 2004; Bronk et al., 2018). Similarly, sei channels were shown to be enriched in axonal projections in glutamatergic and octopaminergic neurons (Hill et al., 2019). Consistent with this, our results indicate that

ziram affects axonal projections more strongly than cell bodies (Fig. 2C, D). However, the increased firing threshold in adult abdominal ganglion cell bodies detected by whole-cell recordings indicates a possible direct effect on cell bodies (Fig. 3B, C).

We hypothesize that ziram will also inhibit eag orthologs in mammalian neurons. Our attention has been particularly drawn to the channel encoded by human *eag*-related gene 1 (hERG1/KCNH2/Kv11.1) because of its relevance to human disease, especially cardiac arrhythmias (Vandenberg et al., 2012). Disruption of hERG1 activity caused by either genetic mutations or drugs is a major cause of long QT syndrome that increases the risk of potentially fatal arrhythmias (Perrin and Gollob, 2013; Perry et al., 2015). Interestingly, the prevalence of long QT syndrome is also elevated in PD patients (Deguchi et al., 2002) and emerging evidence indicates an interaction between arrhythmias and AD (Ihara and Washida, 2018), but the potential relevance of hERG to PD or AD has not been explored. hERG1 is inhibited by an unusually large number of structurally diverse drugs including commonly prescribed drugs and our findings suggest that ziram might be added to this list (Suessbrich et al., 1997; Thomas et al., 2002; Lee et al., 2012; Kratz et al., 2017).

A majority of studies on inhibition of eag orthologs have focused on its physiology in the context of cardiac conditions, but all members of this family are widely expressed in the nervous system (Jeng et al., 2005; Ferreira et al., 2012; Perrin and Gollob, 2013; Perry et al., 2015). We speculate that inhibition of human eag orthologs by ziram and by other compounds increases neuronal excitability and contributes to the initiation of disease and possibly early progression of neurotoxicity (Duda et al., 2016). ERG channels are highly expressed in the striatum, globus pallidus, and SN, and hERG inhibitors (E4031 and rBeKm-1) directly increase the rate of spontaneous firing in midbrain DA neurons (Ferreira et al., 2012; Ji et al., 2012). *eag* orthologs are also expressed in CNS glutamatergic neurons (Jeng et al., 2005; Vandenberg et al., 2012). It is possible that inhibition of a subset of human *eag* channels by ziram could indirectly and directly affect DA neurons by increasing excitatory glutamatergic drive and by increasing DA neuron activity, thus increasing metabolic load (Blandini, 2010; Ji et al., 2012). *eag* orthologs are also expressed in NE neurons and contribute to physiological functions such as heart rate, sleep, arousal, and stress (Gullo et al., 2003; Schwarz and Luo, 2015). We note that in flies, *sei* and *eag* mutants exhibit neuropathology and reduced longevity, suggesting their potential relevance to neurodegenerative diseases (Fergestad et al., 2006). Although the mechanisms underlying these effects remain unclear, these data suggest that additional studies in the fly might be used to dissect the relationship between the eag family and downstream pathophysiological processes.

In summary, we have used *Drosophila* molecular genetics in combination with calcium imaging and electrophysiology to identify target pathways, which may contribute to neurophysiological effects of ziram. If dysfunction of the eag channel family in humans does indeed play a role in human neuropathology, it will necessitate the evaluation of mutations as risk factors, and of additional environmental and pharmaceutical compounds that act on these channels. Our data further suggest that patients exposed to ziram should be examined for evidence of cardiac hyperexcitability, a known risk of drugs that target the eag family of K channels.

Conclusion

Complex diseases such as idiopathic PD are thought to be caused by the interaction of multiple genetic and environmental factors. While the study of genetic risk factors has contributed enormously to our mechanistic understanding of complex diseases, environmental toxicants have received much less attention. We propose that examination of the acute effects of disease-linked environmental factors will expose potentially novel molecular pathways involved in complex diseases. Using *Drosophila*, we show that the widely used agricultural fungicide ziram alters both glutamatergic and aminergic neuronal function via two distinct mechanisms: i) increasing the probability of vesicle release through an E1-ligase dependent pathway and, ii), increasing electrophysiological excitability. Null mutants of the potassium channel *ether a-go-go* phenocopy and occlude the ziram-induced increase in excitability. Moreover, E4031, an inhibitor of the hERG (human *eag* related gene) channel, an ortholog of sei, also phenocopies and occludes ziram-induced excitability increases, but only at elevated temperatures. Sei or a related channel may thus be an additional target of ziram at elevated temperatures. Taken together, our data raise the novel possibility that ziram could inhibit human eag channel orthologs such as hERG and thereby contribute to human disease states such as PD.

Acknowledgments

We thank Stephanie A. White and Jeffrey M. Donlea for insightful comments on the manuscript. We thank Aditya Eamani and Sonali Deshpande for technical help through the study. We also acknowledge the support of many undergraduate students with fly husbandry and experimental help, especially Deepna Chand, Dake Huang and Elise Denghausen.

This work was supported by T32ES015457(JH) NS075506 (FES), MH107390 and MH114017 (DEK)

Abbreviations

AD	Alzheimer’s disease
AP	action potential
DA	dopaminergic
eag	ether a-go-go
erg	ether-a-go-go related gene
EJP	end junction potential
elk	ether-a-go-go like gene
K	potassium
NE	norepinephrine
NMJ	neuromuscular junction
PD	Parkinson’s disease
sei	seizure

TEA	tetraethylammonium
TTX	tetrodotoxin
VNC	ventral nerve cord

References

Ambrosi G, Cerri S, Blandini F (2014) A further update on the role of excitotoxicity in the pathogenesis of Parkinson's disease. J Neural Transm (Vienna) 121:849–859. [PubMed: 24380931]

Ascherio A, Schwarzschild MA (2016) The epidemiology of Parkinson's disease: risk factors and prevention. Lancet Neurol 15:1257–1272. [PubMed: 27751556]

Atwood HL, Govind CK, Wu CF (1993) Differential ultrastructure of synaptic terminals on ventral longitudinal abdominal muscles in Drosophila larvae. J Neurobiol 24:1008–1024. [PubMed: 8409966]

Baltazar MT, Dinis-Oliveira RJ, de Lourdes Bastos M, Tsatsakis AM, Duarte JA, Carvalho F (2014) Pesticides exposure as etiological factors of Parkinson's disease and other neurodegenerative diseases--a mechanistic approach. Toxicol Lett 230:85–103. [PubMed: 24503016]

Bauer CK, Schwarz JR (2018) Ether-a-go-go K(+) channels: effective modulators of neuronal excitability. J Physiol 596:769–783. [PubMed: 29333676]

Bezard E, Yue Z, Kirik D, Spillantini MG (2013) Animal models of Parkinson's disease: limits and relevance to neuroprotection studies. Mov Disord 28:61–70. [PubMed: 22753348]

Blandini F (2010) An update on the potential role of excitotoxicity in the pathogenesis of Parkinson's disease. Funct Neurol 25:65–71. [PubMed: 20923603]

Bronk P, Kuklin EA, Gorur-Shandilya S, Liu C, Wiggin TD, Reed ML, Marder E, Griffith LC (2018) Regulation of Eag by Ca(2+)/calmodulin controls presynaptic excitability in Drosophila. J Neurophysiol 119:1665–1680. [PubMed: 29364071]

Calabresi P, Mercuri NB, Sancesario G, Bernardi G (1993) Electrophysiology of dopamine-denervated striatal neurons. Implications for Parkinson's disease. Brain 116 (Pt 2):433–452. [PubMed: 8096420]

Cannon JR, Greenamyre JT (2011) The role of environmental exposures in neurodegeneration and neurodegenerative diseases. Toxicol Sci 124:225–250. [PubMed: 21914720]

Cao F, Souders Ii CL, Perez-Rodriguez V, Martyniuk CJ (2018) Elucidating Conserved Transcriptional Networks Underlying Pesticide Exposure and Parkinson's Disease: A Focus on Chemicals of Epidemiological Relevance. Front Genet 9:701. [PubMed: 30740124]

Cao F, Souders CL, Li P, Adamovsky O, Pang S, Qiu L, Martyniuk CJ (2019) Developmental toxicity of the fungicide ziram in zebrafish (Danio rerio). Chemosphere 214:303–313. [PubMed: 30265938]

Carvey PM, Punati A, Newman MB (2006) Progressive dopamine neuron loss in Parkinson's disease: the multiple hit hypothesis. Cell Transplant 15:239–250. [PubMed: 16719059]

Chen TW, Wardill TJ, Sun Y, Pulver SR, Renninger SL, Baohan A, Schreiter ER, Kerr RA, Orger MB, Jayaraman V, Looger LL, Svoboda K, Kim DS (2013) Ultrasensitive fluorescent proteins for imaging neuronal activity. Nature 499:295–300. [PubMed: 23868258]

Chen X, Xue B, Wang J, Liu H, Shi L, Xie J (2018) Potassium Channels: A Potential Therapeutic Target for Parkinson's Disease. Neurosci Bull 34:341–348. [PubMed: 28884460]

Chou AP, Maidment N, Klintenberg R, Casida JE, Li S, Fitzmaurice AG, Fernagut PO, Mortazavi F, Chesselet MF, Bronstein JM (2008) Ziram causes dopaminergic cell damage by inhibiting E1 ligase of the proteasome. J Biol Chem 283:34696–34703. [PubMed: 18818210]

Cole SH, Carney GE, McClung CA, Willard SS, Taylor BJ, Hirsh J (2005) Two functional but noncomplementing Drosophila tyrosine decarboxylase genes: distinct roles for neural tyramine and octopamine in female fertility. J Biol Chem 280:14948–14955. [PubMed: 15691831]

Cosselman KE, Navas-Acien A, Kaufman JD (2015) Environmental factors in cardiovascular disease. Nat Rev Cardiol 12:627–642. [PubMed: 26461967]

de Lau LM, Breteler MM (2006) Epidemiology of Parkinson's disease. Lancet Neurol 5:525–535. [PubMed: 16713924]

De Strooper B, Karran E (2016) The Cellular Phase of Alzheimer's Disease. Cell 164:603–615. [PubMed: 26871627]

Deguchi K, Sasaki I, Tsukaguchi M, Kamoda M, Touge T, Takeuchi H, Kuriyama S (2002) Abnormalities of rate-corrected QT intervals in Parkinson's disease-a comparison with multiple system atrophy and progressive supranuclear palsy. J Neurol Sci 199:31–37. [PubMed: 12084439]

Dennis KE, Valentine WM (2015) Ziram and sodium N,N-dimethyldithiocarbamate inhibit ubiquitin activation through intracellular metal transport and increased oxidative stress in HEK293 cells. Chem Res Toxicol 28:682–690. [PubMed: 25714994]

DiAntonio A, Hicke L (2004) Ubiquitin-dependent regulation of the synapse. Annu Rev Neurosci 27:223–246. [PubMed: 15217332]

Dragicevic E, Schiemann J, Liss B (2015) Dopamine midbrain neurons in health and Parkinson's disease: emerging roles of voltage-gated calcium channels and ATP-sensitive potassium channels. Neuroscience 284:798–814. [PubMed: 25450964]

Duda J, Potschke C, Liss B (2016) Converging roles of ion channels, calcium, metabolic stress, and activity pattern of Substantia nigra dopaminergic neurons in health and Parkinson's disease. J Neurochem 139 Suppl 1:156–178. [PubMed: 26865375]

Efron B, Tibshirani R (1991) Statistical data analysis in the computer age. Science 253:390–395. [PubMed: 17746394]

Efron B, Hastie T (2016) Computer Age Statistical Inference: Algorithms, Evidence, and Data Science Cambridge Univ. Press.

Feng Y, Ueda A, Wu CF (2004) A modified minimal hemolymph-like solution, HL3.1, for physiological recordings at the neuromuscular junctions of normal and mutant Drosophila larvae. J Neurogenet 18:377–402. [PubMed: 15763995]

Fergestad T, Ganetzky B, Palladino M (2006) Neuropathology in Drosophila Membrane Excitability Mutants. Genetics 172:1031–1042. [PubMed: 16272407]

Ferreira NR, Mitkovski M, Stuhmer W, Pardo LA, Del Bel EA (2012) Ether-a-go-go 1 (Eag1) potassium channel expression in dopaminergic neurons of basal ganglia is modulated by 6-hydroxydopamine lesion. Neurotoxicity research 21:317–333. [PubMed: 22048886]

Fitzmaurice AG, Rhodes SL, Cockburn M, Ritz B, Bronstein JM (2014) Aldehyde dehydrogenase variation enhances effect of pesticides associated with Parkinson disease. Neurology 82:419–426. [PubMed: 24491970]

Fox LE, Soll DR, Wu CF (2006) Coordination and modulation of locomotion pattern generators in Drosophila larvae: effects of altered biogenic amine levels by the tyramine beta hydroxlyase mutation. J Neurosci 26:1486–1498. [PubMed: 16452672]

Frolov RV, Bagati A, Casino B, Singh S (2012) Potassium channels in Drosophila: historical breakthroughs, significance, and perspectives. J Neurogenet 26:275–290. [PubMed: 23181728]

Ganetzky B, Wu CF (1983) Neurogenetic analysis of potassium currents in Drosophila: synergistic effects on neuromuscular transmission in double mutants. J Neurogenet 1:17–28. [PubMed: 6100303]

Ganetzky B, Wu CF (1986) Neurogenetics of membrane excitability in Drosophila. Annu Rev Genet 20:13–44. [PubMed: 2434020]

Ganetzky B, Robertson GA, Wilson GF, Trudeau MC, Titus SA (1999) The eag family of K+ channels in Drosophila and mammals. Ann N Y Acad Sci 868:356–369. [PubMed: 10414305]

Goldman SM (2014) Environmental toxins and Parkinson's disease. Annual review of pharmacology and toxicology 54:141—164.

Goldman SM, Kamel F, Ross GW, Bhudhikanok GS, Hoppin JA, Korell M, Marras C, Meng C, Umbach DM, Kasten M, Chade AR, Comyns K, Richards MB, Sandler DP, Blair A, Langston JW, Tanner CM (2012) Genetic modification of the association of paraquat and Parkinson's disease. Mov Disord 27:1652–1658. [PubMed: 23045187]

Gullo F, Ales E, Rosati B, Lecchi M, Masi A, Guasti L, Cano-Abad MF, Arcangeli A, Lopez MG, Wanke E (2003) ERG K+ channel blockade enhances firing and epinephrine secretion in rat

chromaffin cells: the missing link to LQT2-related sudden death? FASEB J 17:330–332. [PubMed: 12490549]

Hales KG, Korey CA, Larracuente AM, Roberts DM (2015) Genetics on the Fly: A Primer on the Drosophila Model System. Genetics 201:815–842. [PubMed: 26564900]

Hartmann S, Zheng F, Kyncl MC, Karch S, Voelkl K, Zott B, D'Avanzo C, Lomoio S, Tesco G, Kim DY, Alzheimer C, Huth T (2018) beta-Secretase BACE1 Promotes Surface Expression and Function of Kv3.4 at Hippocampal Mossy Fiber Synapses. J Neurosci 38:3480–3494. [PubMed: 29507146]

Heinemann SD, Posimo JM, Mason DM, Hutchison DF, Leak RK (2016) Synergistic stress exacerbation in hippocampal neurons: Evidence favoring the dual-hit hypothesis of neurodegeneration. Hippocampus 26:980–994. [PubMed: 26934478]

Hill AS, Jain P, Folan NE, Ben-Shahar Y (2019) The Drosophila ERG channel seizure plays a role in the neuronal homeostatic stress response. PLoS Genet 15:e1008288.

Ihara M, Washida K (2018) Linking Atrial Fibrillation with Alzheimer's Disease: Epidemiological, Pathological, and Mechanistic Evidence. J Alzheimers Dis 62:61–72. [PubMed: 29439352]

Imlach W, McCabe BD (2009) Electrophysiological Methods for Recording Synaptic Potentials from the NMJ of Drosophila Larvae. JoVE:e1109.

Jackson FR, Wilson SD, Strichartz GR, Hall LM (1984) Two types of mutants affecting voltage-sensitive sodium channels in Drosophila melanogaster. Nature 308:189–191. [PubMed: 6322008]

Jan LY, Jan YN (2012) Voltage-gated potassium channels and the diversity of electrical signalling. J Physiol 590:2591–2599. [PubMed: 22431339]

Jeng CJ, Chang CC, Tang CY (2005) Differential localization of rat Eag1 and Eag2 K+ channels in hippocampal neurons. Neuroreport 16:229–233. [PubMed: 15706225]

Ji H, Tucker KR, Putzier I, Huertas MA, Horn JP, Canavier CC, Levitan ES, Shepard PD (2012) Functional characterization of ether-a-go-go-related gene potassium channels in midbrain dopamine neurons - implications for a role in depolarization block. Eur J Neurosci 36:2906–2916. [PubMed: 22780096]

Jin J, Lao AJ, Katsura M, Caputo A, Schweizer FE, Sokolow S (2014) Involvement of the sodium-calcium exchanger 3 (NCX3) in ziram-induced calcium dysregulation and toxicity. Neurotoxicology 45:56–66. [PubMed: 25284465]

Koon AC, Budnik V (2012) Inhibitory control of synaptic and behavioral plasticity by octopaminergic signaling. J Neurosci 32:6312–6322. [PubMed: 22553037]

Kratz JM, Grienke U, Scheel O, Mann SA, Rollinger JM (2017) Natural products modulating the hERG channel: heartaches and hope. Nat Prod Rep 34:957–980. [PubMed: 28497823]

Kutsukake M, Komatsu A, Yamamoto D, Ishiwa-Chigusa S (2000) A tyramine receptor gene mutation causes a defective olfactory behavior in Drosophila melanogaster. Gene 245:31–42. [PubMed: 10713442]

Langston JW (2017) The MPTP Story. J Parkinsons Dis 7:S11–s19. [PubMed: 28282815]

Lee J, Wu CF (2010) Orchestration of Stepwise Synaptic Growth by K+ and Ca2+ Channels in Drosophila. J Neurosci 30(47):15821–15833. [PubMed: 21106821]

Lee SH, Sung MJ, Hahn SJ, Kim J, Min G, Jo SH, Choe H, Choi BH (2012) Blockade of human HERG K(+) channels by rosiglitazone, an antidiabetic drug. Arch Pharm Res 35:1655–1664. [PubMed: 23054723]

Lehnert S, Hartmann S, Hessler S, Adelsberger H, Huth T, Alzheimer C (2016) Ion channel regulation by beta-secretase BACE1 - enzymatic and non-enzymatic effects beyond Alzheimer's disease. Channels (Austin) 10:365–378. [PubMed: 27253079]

Liss B, Haeckel O, Wildmann J, Miki T, Seino S, Roeper J (2005) K-ATP channels promote the differential degeneration of dopaminergic midbrain neurons. Nat Neurosci 8:1742–1751. [PubMed: 16299504]

Littleton JT, Ganetzky B (2000) Ion channels and synaptic organization: analysis of the Drosophila genome. Neuron 26:35–43. [PubMed: 10798390]

Lotharius J, Brundin P (2002) Pathogenesis of Parkinson's disease: dopamine, vesicles and alpha-synuclein. Nat Rev Neurosci 3:932–942. [PubMed: 12461550]

Mackay TF (2015) Epistasis for quantitative traits in Drosophila. Methods Mol Biol 1253:47–70. [PubMed: 25403527]

Martin CA, Myers KM, Chen A, Martin NT, Barajas A, Schweizer FE, Krantz DE (2016) Ziram, a pesticide associated with increased risk for Parkinson's disease, differentially affects the presynaptic function of aminergic and glutamatergic nerve terminals at the Drosophila neuromuscular junction. Exp Neurol 275 Pt 1:232–241. [PubMed: 26439313]

Matei AM, Trombetta LD (2016) Exposure of rat hippocampal astrocytes to Ziram increases oxidative stress. Toxicol Ind Health 32:579–588. [PubMed: 24193059]

Mauerhöfer M, Bauer CK (2016) Effects of Temperature on Heteromeric Kv11.1a/1b and Kv11.3 Channels. Biophys J 111:504–523. [PubMed: 27508435]

McCormack AL, Thiruchelvam M, Manning-Bog AB, Thiffault C, Langston JW, Cory-Slechta DA, Di Monte DA (2002) Environmental risk factors and Parkinson's disease: selective degeneration of nigral dopaminergic neurons caused by the herbicide paraquat. Neurobiol Dis 10:119–127. [PubMed: 12127150]

Monastirioti M, Gorczyca M, Rapus J, Eckert M, White K, Budnik V (1995) Octopamine immunoreactivity in the fruit fly Drosophila melanogaster. J Comp Neurol 356:275–287. [PubMed: 7629319]

Mostafalou S, Abdollahi M (2013) Pesticides and human chronic diseases: evidences, mechanisms, and perspectives. Toxicol Appl Pharmacol 268:157–177. [PubMed: 23402800]

Muddapu VR, Mandali A, Chakravarthy VS, Ramaswamy S (2019) A Computational Model of Loss of Dopaminergic Cells in Parkinson's Disease Due to Glutamate-Induced Excitotoxicity. Front Neural Circuits 13:11. [PubMed: 30858799]

Nagaya Y, Kutsukake M, Chigusa SI, Komatsu A (2002) A trace amine, tyramine, functions as a neuromodulator in Drosophila melanogaster. Neurosci Lett 329:324–328. [PubMed: 12183041]

Nandipati S, Litvan I (2016) Environmental Exposures and Parkinson's Disease. Int J Environ Res Public Health 13.

Noyce AJ, Lees AJ, Schrag A-E (2016) The prediagnostic phase of Parkinson's disease. Journal of Neurology, Neurosurgery & Psychiatry 87:871–878.

Ocorr K, Zambon A, Nudell Y, Pineda S, Diop S, Tang M, Akasaka T, Taylor E (2017) Age-dependent electrical and morphological remodeling of the Drosophila heart caused by hERG/seizure mutations. In: PLoS Genet.

Pallanck L, Ganetzky B (1994) Cloning and characterization of human and mouse homologs of the Drosophila calcium-activated potassium channel gene, slowpoke. Hum Mol Genet 3:1239–1243. [PubMed: 7987297]

Parron T, Requena M, Hernandez AF, Alarcon R (2011) Association between environmental exposure to pesticides and neurodegenerative diseases. Toxicol Appl Pharmacol 256:379–385. [PubMed: 21601587]

Perrin MJ, Gollob MH (2013) Genetics of cardiac electrical disease. Can J Cardiol 29:89–99. [PubMed: 23062665]

Perry MD, Ng CA, Mann SA, Sadrieh A, Imtiaz M, Hill AP, Vandenberg JI (2015) Getting to the heart of hERG K(+) channel gating. The Journal of physiology 593:2575–2585. [PubMed: 25820318]

Ramachandran KV, Margolis SS (2017) A mammalian nervous-system-specific plasma membrane proteasome complex that modulates neuronal function. Nat Struct Mol Biol 24:419–430. [PubMed: 28287632]

Ramachandran KV, Fu JM, Schaffer TB, Na CH, Delannoy M, Margolis SS (2018) Activity-Dependent Degradation of the Nascentome by the Neuronal Membrane Proteasome. Mol Cell 71:169–177.e166.

Rezaval C, Pavlou HJ, Dornan AJ, Chan YB, Kravitz EA, Goodwin SF (2012) Neural circuitry underlying Drosophila female postmating behavioral responses. Curr Biol 22:1155–1165. [PubMed: 22658598]

Ridding MC, Inzelberg R, Rothwell JC (1995) Changes in excitability of motor cortical circuitry in patients with Parkinson's disease. Ann Neurol 37:181–188. [PubMed: 7847860]

Rinetti GV, Schweizer FE (2010) Ubiquitination acutely regulates presynaptic neurotransmitter release in mammalian neurons. J Neurosci 30:3157–3166. [PubMed: 20203175]

Rodriguez-Valentin R, Lopez-Gonzalez I, Jorquera R, Labarca P, Zurita M, Reynaud E (2006) Oviduct contraction in Drosophila is modulated by a neural network that is both, octopaminergic and glutamatergic. J Cell Physiol 209:183–198. [PubMed: 16826564]

Ryglewski S, Duch C (2012) Preparation of Drosophila Central Neurons for in situ Patch Clamping. In: J Vis Exp.

Saraswati S, Fox LE, Soll DR, Wu CF (2004) Tyramine and octopamine have opposite effects on the locomotion of Drosophila larvae. J Neurobiol 58:425–441. [PubMed: 14978721]

Schwarz LA, Luo L (2015) Organization of the Locus Coeruleus-Norepinephrine System. Curr Biol 25:R1051–R1056. [PubMed: 26528750]

Selcho M, Pauls D, Huser A, Stocker RF, Thum AS (2014) Characterization of the octopaminergic and tyraminergic neurons in the central brain of Drosophila larvae. J Comp Neurol 522:3485–3500. [PubMed: 24752702]

Shieh CC, Coghlan M, Sullivan JP, Gopalakrishnan M (2000) Potassium channels: molecular defects, diseases, and therapeutic opportunities. Pharmacol Rev 52:557–594. [PubMed: 11121510]

Simon AF, Daniels R, Romero-Calderón R, Grygoruk A, Chang HY, Najibi R, Shamouelian D, Salazar E, Solomon M, Ackerson LC, Maidment NT, DiAntonio A, Krantz DE (2009) Drosophila Vesicular Monoamine Transporter Mutants Can Adapt to Reduced or Eliminated Vesicular Stores of Dopamine and Serotonin. In: Genetics, pp 525–541. [PubMed: 19033154]

Speese SD, Trotta N, Rodesch CK, Aravamudan B, Broadie K (2003) The ubiquitin proteasome system acutely regulates presynaptic protein turnover and synaptic efficacy. Curr Biol 13:899–910. [PubMed: 12781128]

Stallones L, Beseler CL (2016) Assessing the connection between organophosphate pesticide poisoning and mental health: A comparison of neuropsychological symptoms from clinical observations, animal models and epidemiological studies. Cortex 74:405–416. [PubMed: 26654853]

Subramaniam M, Althof D, Gispert S, Schwenk J, Auburger G, Kulik A, Fakler B, Roeper J (2014) Mutant alpha-synuclein enhances firing frequencies in dopamine substantia nigra neurons by oxidative impairment of A-type potassium channels. J Neurosci 34:13586–13599. [PubMed: 25297088]

Suessbrich H, Schonherr R, Heinemann SH, Attali B, Lang F, Busch AE (1997) The inhibitory effect of the antipsychotic drug haloperidol on HERG potassium channels expressed in Xenopus oocytes. Br J Pharmacol 120:968–974. [PubMed: 9138706]

Sulzer D (2007) Multiple hit hypotheses for dopamine neuron loss in Parkinson's disease. Trends Neurosci 30:244–250. [PubMed: 17418429]

Sun XX, Hodge JJ, Zhou Y, Nguyen M, Griffith LC (2004) The eag potassium channel binds and locally activates calcium/calmodulin-dependent protein kinase II. J Biol Chem 279:10206–10214. [PubMed: 14699099]

Szot P (2012) Common factors among Alzheimer's disease, Parkinson's disease, and epilepsy: Possible role of the noradrenergic nervous system. Epilepsia 53:61—66. [PubMed: 22612810]

Thomas D, Gut B, Wendt-Nordahl G, Kiehn J (2002) The antidepressant drug fluoxetine is an inhibitor of human ether-a-go-go-related gene (HERG) potassium channels. J Pharmacol Exp Ther 300:543–548. [PubMed: 11805215]

Titus SA, Warmke JW, Ganetzky B (1997) The Drosophila erg K+ channel polypeptide is encoded by the seizure locus. J Neurosci 17:875–881. [PubMed: 8994042]

Vandenberg JI, Varghese A, Lu Y, Bursill JA, Mahaut-Smith MP, Huang CL (2006) Temperature dependence of human ether-a-go-go-related gene K+ currents. Am J Physiol Cell Physiol 291:C165–175. [PubMed: 16452156]

Vandenberg JI, Perry MD, Perrin MJ, Mann SA, Ke Y, Hill AP (2012) hERG K(+) channels: structure, function, and clinical significance. Physiol Rev 92:1393–1478. [PubMed: 22988594]

Wang A, Costello S, Cockburn M, Zhang X, Bronstein J, Ritz B (2011) Parkinson's disease risk from ambient exposure to pesticides. Eur J Epidemiol 26:547–555. [PubMed: 21505849]

Wang XJ, Reynolds ER, Deak P, Hall LM (1997) The seizure locus encodes the Drosophila homolog of the HERG potassium channel. J Neurosci 17:882–890. [PubMed: 8994043]

Xing X, Wu CF (2018) Unraveling Synaptic GCaMP Signals: Differential Excitability and Clearance Mechanisms Underlying Distinct Ca2+ Dynamics in Tonic and Phasic Excitatory, and Aminergic Modulatory Motor Terminals in Drosophila. In: eNeuro.

Yegambaram M, Manivannan B, Beach TG, Halden RU (2015) Role of environmental contaminants in the etiology of Alzheimer's disease: a review. Curr Alzheimer Res 12:116–146. [PubMed: 25654508]

Yi JJ, Ehlers MD (2005) Ubiquitin and protein turnover in synapse function. Neuron 47:629–632. [PubMed: 16129392]

Zheng X, Valakh V, Diantonio A, Ben-Shahar Y (2014) Natural antisense transcripts regulate the neuronal stress response and excitability. Elife 3:e01849.

Zott B, Busche MA, Sperling RA, Konnerth A (2018) What Happens with the Circuit in Alzheimer's Disease in Mice and Humans? Annu Rev Neurosci 41:277–297. [PubMed: 29986165]

Highlights

- The neurotoxicant ziram disrupts neuronal activity via two distinct mechanisms
- Mechanism 1: increased synaptic release by inhibition of the ubiquitin signaling system
- Mechanism 2: increased excitability by inhibition of the eag family of K channels
- Both pathways may contribute to human disease
- Environmental toxicants can identify novel disease pathways

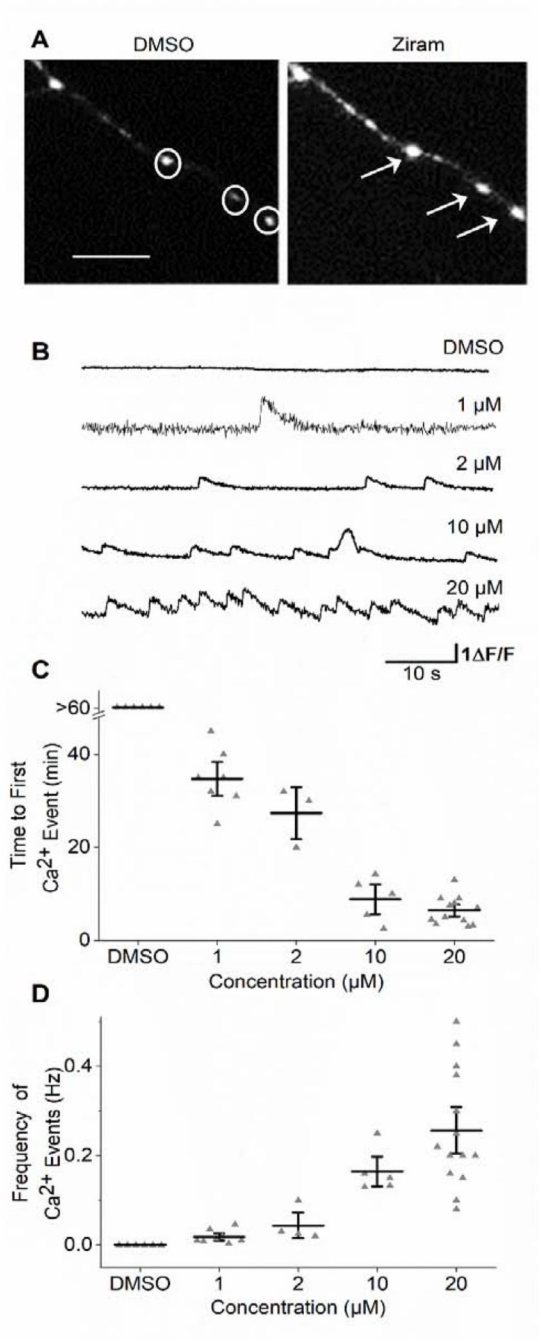

Figure 1. Exposure to ziram dose-dependently increases calcium events at octopaminergic terminals at the NMJ.

A. GCaMP6m fluorescence in muscle 13 at octopaminergic terminals exposed to control solution (left) and the same preparation in 20 μM ziram (right). Regions of interest (ROI) selected for analysis indicated as white circles (left). Note the increase in fluorescence (white arrows; right). Scale bar= 80 μm **B.** Representative ΔF/F traces show repetitive calcium events recorded from octopaminergic terminals after 25 minute exposure to control solution (n=6), 1 μM ziram (n=7), 2 μM ziram (n=4), 10 μM ziram (n=5), or 20 μM ziram (n=15). **C.** The time until the first calcium event decreases as the concentration of ziram

increases with the onset of EJPs occurring earlier at the high doses. **D.** The mean frequency of calcium events at 25–30 minutes post-ziram at each concentration. Data shown as mean ± SEM.

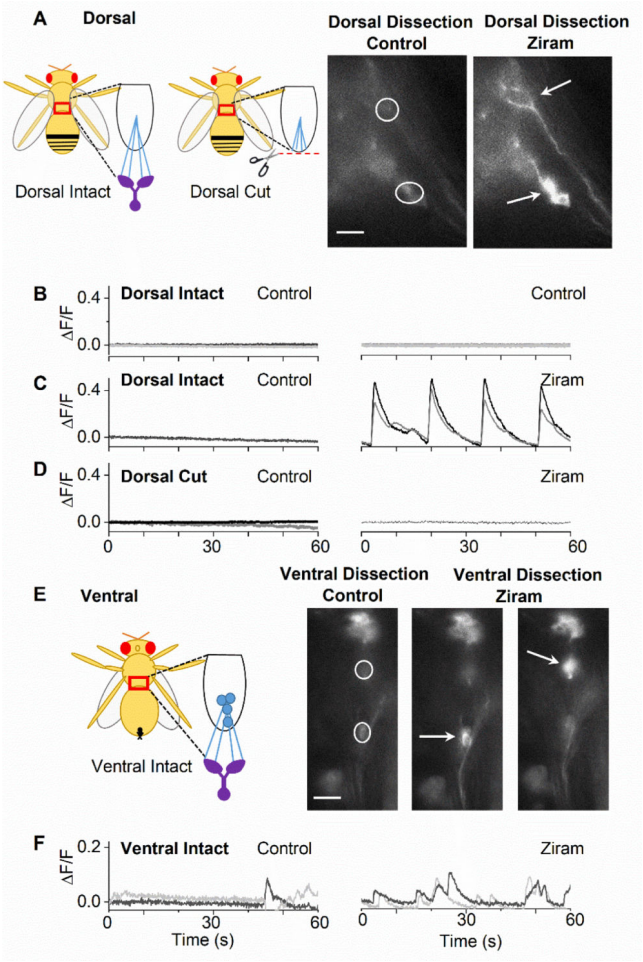

Figure 2. Ziram increases calcium events in octopaminergic projections and somata in the adult abdominal ganglion.

A. Diagram of the dorsal intact and cut abdominal ganglion dissection (*left*): the area within the red square in the fly is shown magnified in the cartoon to the right of fly. Black half-oval: abdominal ganglion; blue lines: octopaminergic projections; purple: target organs of projections. Images of octopaminergic neuronal projections in the dorsally dissected abdominal ganglion (*right*) in the of control period (*left micrograph*) and after application of 20 μM ziram (*right micrograph*). White circles indicate ROI. Note the synchronized calcium events at the octopaminergic projections indicated with white arrows. Scale bar is 160 μm. **B-C.** Representative ΔF/F traces of octopaminergic projections from two ROIs in an intact dorsal preparation in the presence of control at 2 minutes (*left*) and after a 25-minute control solution (B, *right,* n=5) or ziram (C, *right*, n=6) incubation. Each trace represents one ROI as indicated in the dorsal intact preparation shown in diagram A (white circles). **D.** Representative ΔF/F traces of octopaminergic projections from a dorsal cut preparation before (*left, n=5*) and after a 25-minute incubation in 20 μM ziram (*right*, n=5). Each trace represents one ROI in a dorsal cut preparation. Note that ziram no longer leads to synchronized calcium events. **E.** Diagram of the ventral intact abdominal ganglion dissection and fluorescent images of octopaminergic cell bodies in control solution (*left*) and after a 20-minute incubation in 20 μM ziram (*middle and right, images taken approximately*

15 seconds apart). White arrows indicate ziram-induced calcium events that occur in two different cell clusters at two different time points. Scale bar is 160 μm. **F.** Representative ΔF/F traces of calcium events at the indicated ROIs in control (*left*) and after a 20-minute incubation in 20 μM ziram (right, n=3) in a ventral intact preparation. Traces are from the indicated ROIs in diagram E (white circles).

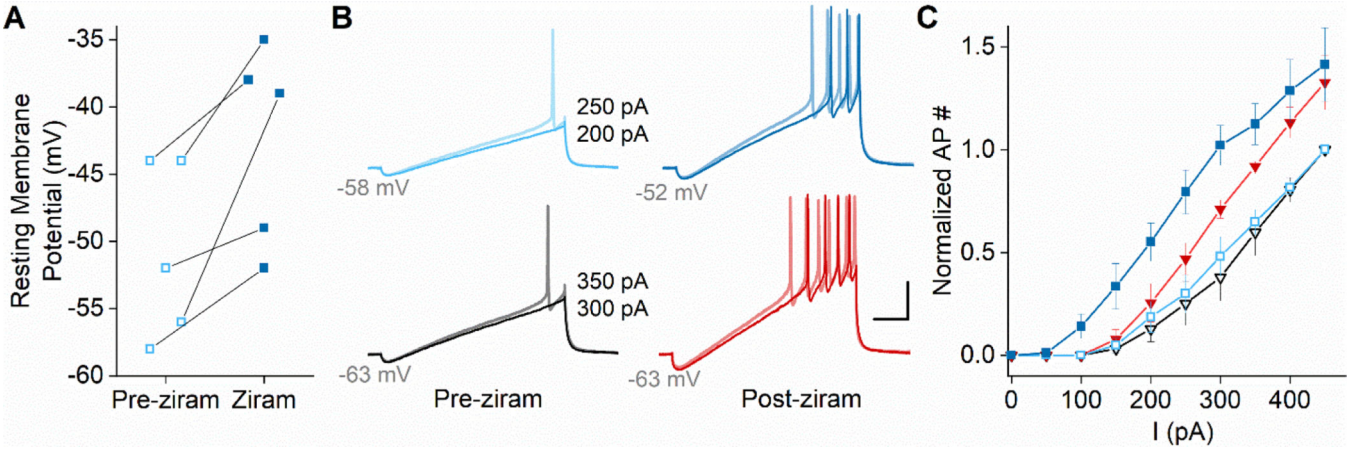

Figure 3. Ziram increases excitability of octopaminergic neurons via depolarization and lowering of AP threshold.

Whole-cell current clamp recordings from octopaminergic neurons in the adult abdominal ganglia before and after perfusion of 10 μM ziram. **A.** Mean resting membrane potential (RP) is depolarized from −51 ± 3 mV to −43 ± 3 mV in the presence of ziram (open light blue squares: control; closed dark blue squares: ziram; n=5). **B.** Representative voltage traces from an individual cell in response to 1 second current ramp injections from −50 pA to 200 or 250 pA (top blue traces) and −50 pA to 300 or 350 pA (bottom black/red traces). Top traces at the cell's resting potential (RP; no bias current) and bottom traces at −63 mV (with bias current) in control (*left*) and 10 μm ziram (*right*). Note that ziram leads to both membrane depolarization and increased AP firing (*top*) and increased AP firing even when the cell is held at −63 mV (*bottom*). Scale bar is 200 ms and 20 mV. **C.** Normalized number of APs in response to 1 second ramp injections from −50 pA to the maximum current indicated on the x-axis. Data are normalized to the pre-ziram AP number for a ramp from −50pA to 450pA (13 APs for RP, 11APs at −63mV). Open symbols: control solution; closed symbols: ziram. Blue (corresponding to blue traces in panel B): neurons at intrinsic RP; Black/red (corresponding to red/black traces in panel B): neurons held at −63 mV with bias current. Mean ± SEM; data from the same 5 cells as shown in A and B. Note the leftward shifts in AP numbers when the cell is in ziram at its RP (light blue to dark blue) and when the potential is held at −63 mV (black to red).

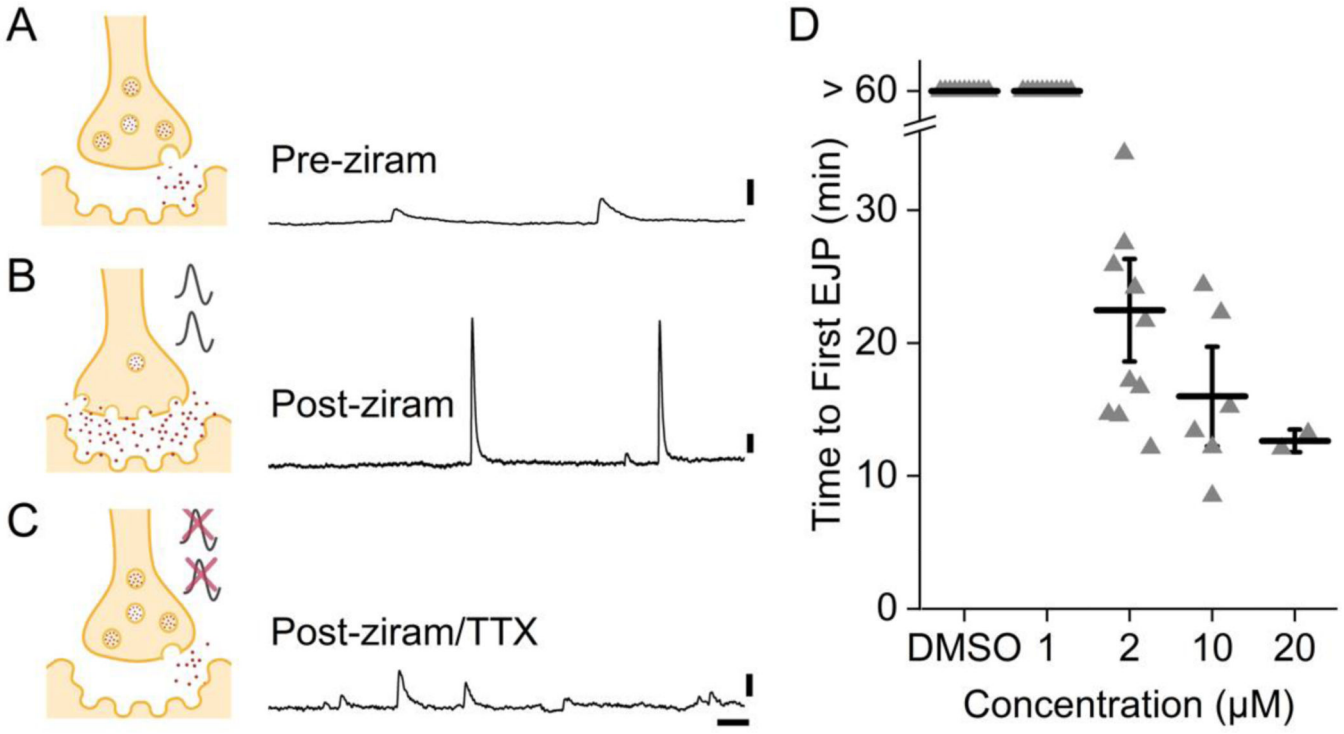

Figure 4. Ziram induces spontaneous, TTX sensitive EJPs at NMJ preparations without VNC.

A- C. Representative trace in control (A, n=11), after addition of 2 μM ziram (B, n=11) and after addition of 1 μM TTX + 2 μM ziram (C, n=4) in preparations without VNC. **A- C.** Scale is 100 ms and 1 mV. **D.** Summary scatter graph of ziram induced EJPs. EJPs are induced at 2, 10, and 20 μM but not at 1 μM or in control solution. Dose of ziram is inversely related to the time to first EJP (Control n=11; 1 μM n=7; 2 μM n=11; 10 μM n=6; 20 μM n=2).

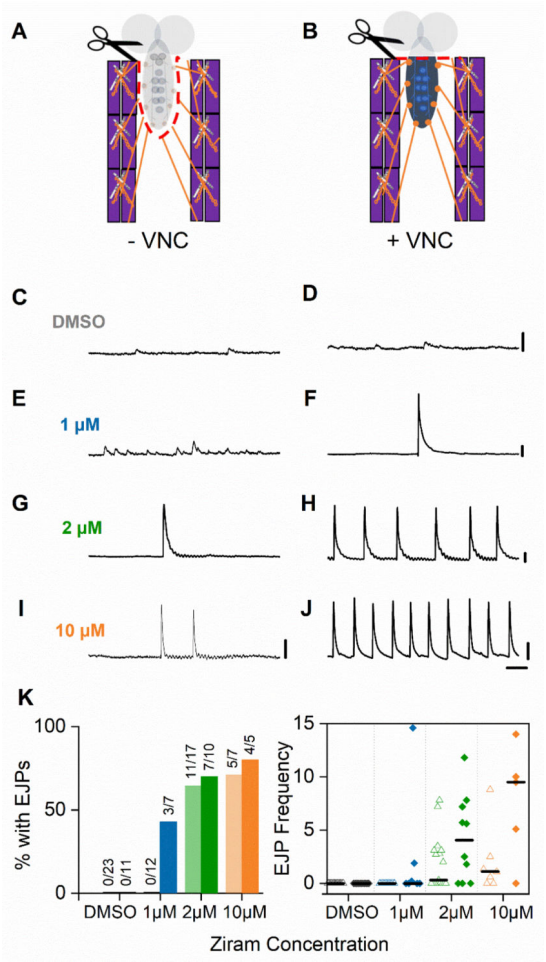

Figure 5. NMJ preparations containing octopaminergic and motor-neuron cell bodies in the VNC are more sensitive to ziram-induced excitability.

A. Diagram depicting the NMJ preparation without the VNC (-VNC) and **B.** with the VNC intact (+VNC). Red dashed lines indicate location of dissection cuts. Blue dots represent octopaminergic cells and orange dots represent glutamatergic motoneuron cell bodies. **C-J.** Representative traces of minis and EJPS in different conditions. **C, E, G: -VNC C.** Control (n=23); **E.** 1 μM ziram (n=12); **G.** 2 μM ziram (n=17); **I.** 10 μM ziram (n=7). **D, F, H: +VNC: D.** Control (n=11); **F.** 1 μM ziram (n=7); **H.** 2 μM ziram (n=10); **J.** 10 μM ziram (n=5). **K.** *Left*: Percentage of experiments with EJPs elicited by ziram during the recording period at each ziram concentration in preparations without (translucent color) and with (bold color) the VNC intact. Note that at 1 μM ziram, EJPs occur only in preparations with the VNC. *Right*: Median frequencies for each experiment in control (grey) and at each ziram dose (blue 1 μM, green 2 μM, orange 10 μM) in preparations with the VNC removed (open triangles) and VNC intact (filled diamonds). Difference of means and confidence interval [5%, 95%]: 1 μM 2.39 [0.03, 6.3]; 2 μM 2.32 [1.4, 4.6] 10 μM 6.24 [2.5, 9.8]; probability of means being equal: 1 μM $p < 0.03$, 2 μM $p < 0.01$, 10 μM $p < 0.001$ (see methods).
Note the increase in frequency when ziram is applied to preparations with the VNC left intact. **C-J.** X scale is 100 ms. **C-F**. Y scale is 1 mV. **G-I.** Y scale is 5 mV**. J.** Y scale is 2 mV.

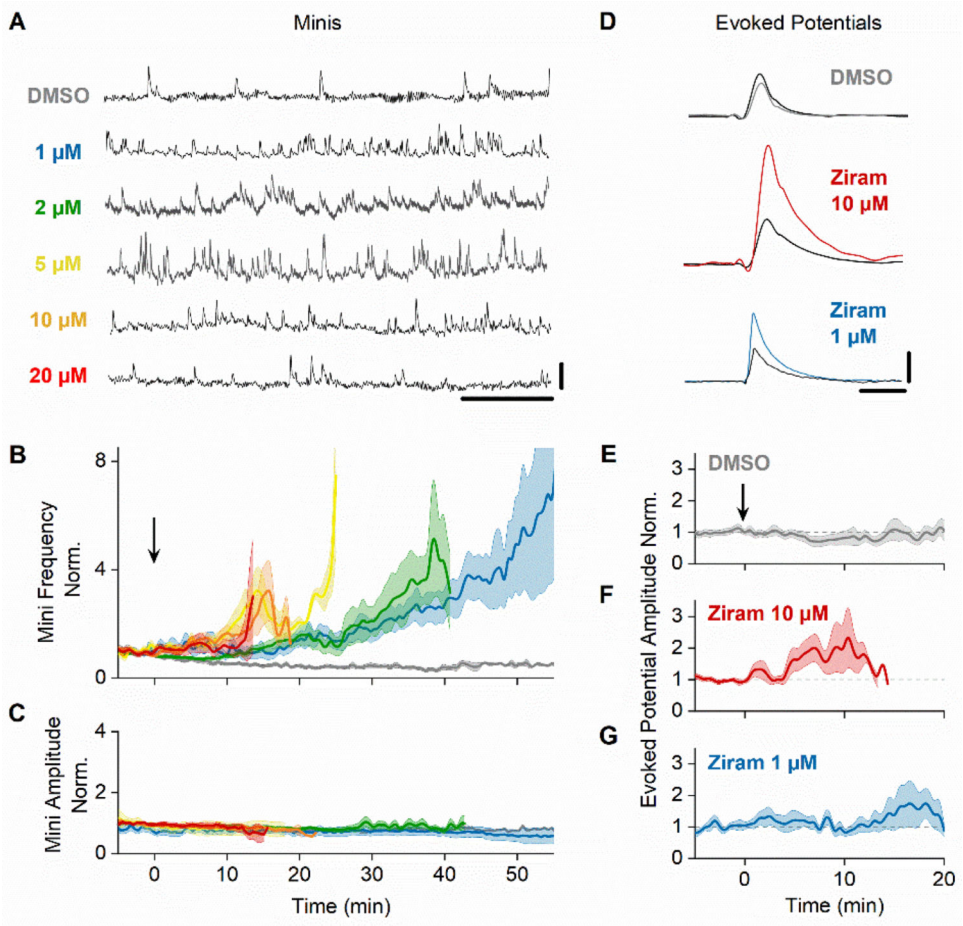

Figure 6. Ziram increases synaptic vesicle release probability.

A. Representative traces of sharp electrode intracellular recordings at the *Drosophila* NMJ in control (grey, n=28) or ziram (blue 1 µM; green 2 µM; yellow 5 µM; orange 10 µM; red 20 µM; n=11–26). X scale is 1 s and Y scale is 0.5 mV. **B, C.** Mini frequency and amplitude measured over time and averaged across experiments in control and in various ziram concentrations. Mini frequencies at 10 µM and 1 µM include experiments performed in both 2 mM and 0.2 mM calcium control solutions. Arrow indicates switch of perfusion from control to drug (or from control to control) solution after a five-minute baseline period. **D.** Sample traces of evoked responses during baseline and after control (grey), 10 µm ziram (red) or 1 µm ziram (blue). Scale is 100 ms and 5 mV. **E-G.** Normalized evoked potential amplitudes plotted over time in control solution (n=8), 10 µM (n=8), and 1 µM ziram (n=5) with addition of drug indicated by black arrow. All time traces are plotted as mean ± SE.

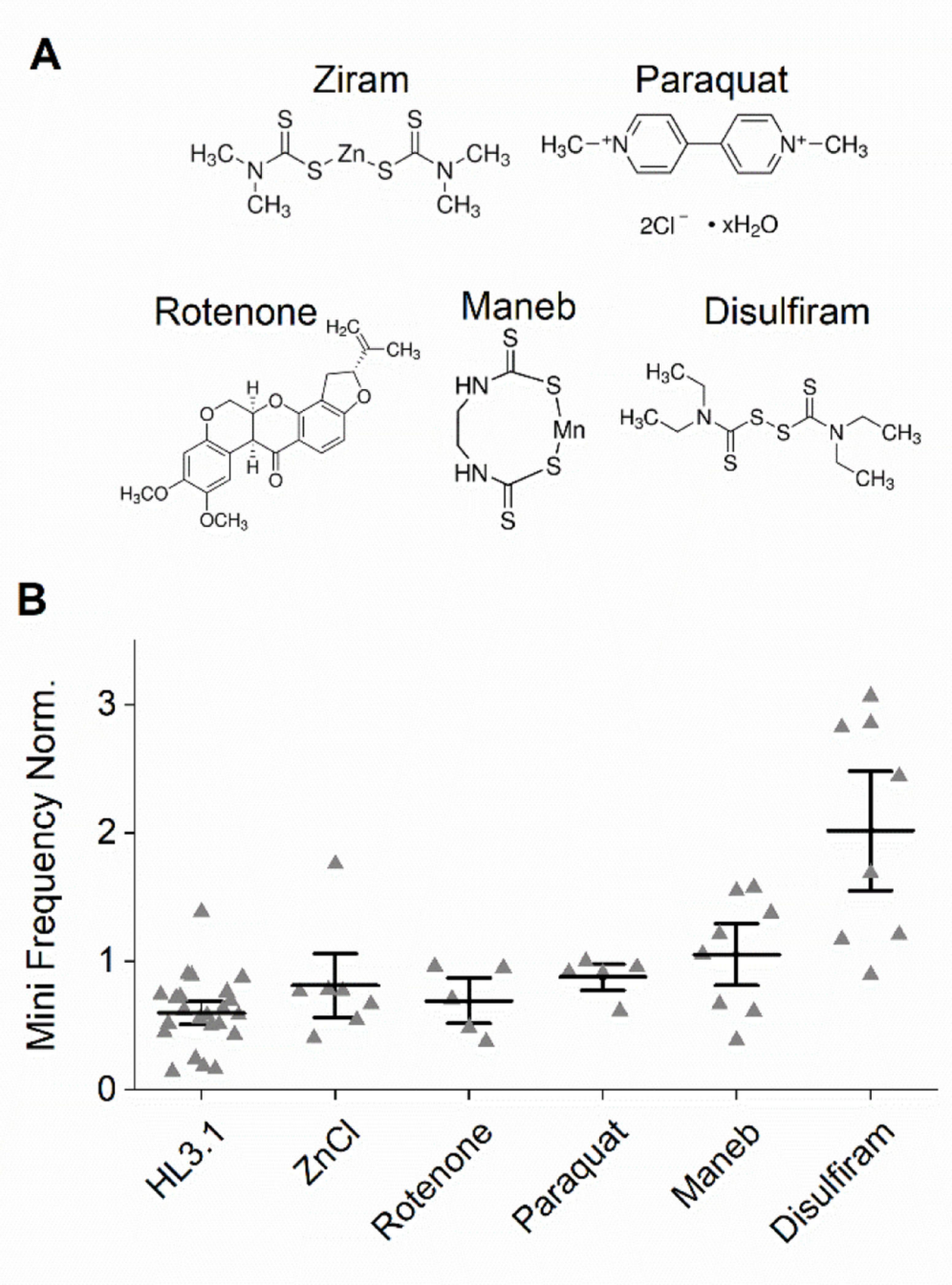

Figure 7. Other PD-associated pesticides, dithiocarbamates, and zinc do not mimic either of the neuronal effects caused by ziram at the NMJ

A. Chemical structures of compounds tested. **B.** Mean mini frequencies in control (n=26), zinc chloride (10 μM, n=8), rotenone (20 μM, n=5), paraquat (20 μM, n=5), maneb (10 μM, n=8) and disulfiram (10 μM, n=8). Disulfiram, and not the other compounds tested, increased mini frequency. None of the compounds tested induce EJPs.

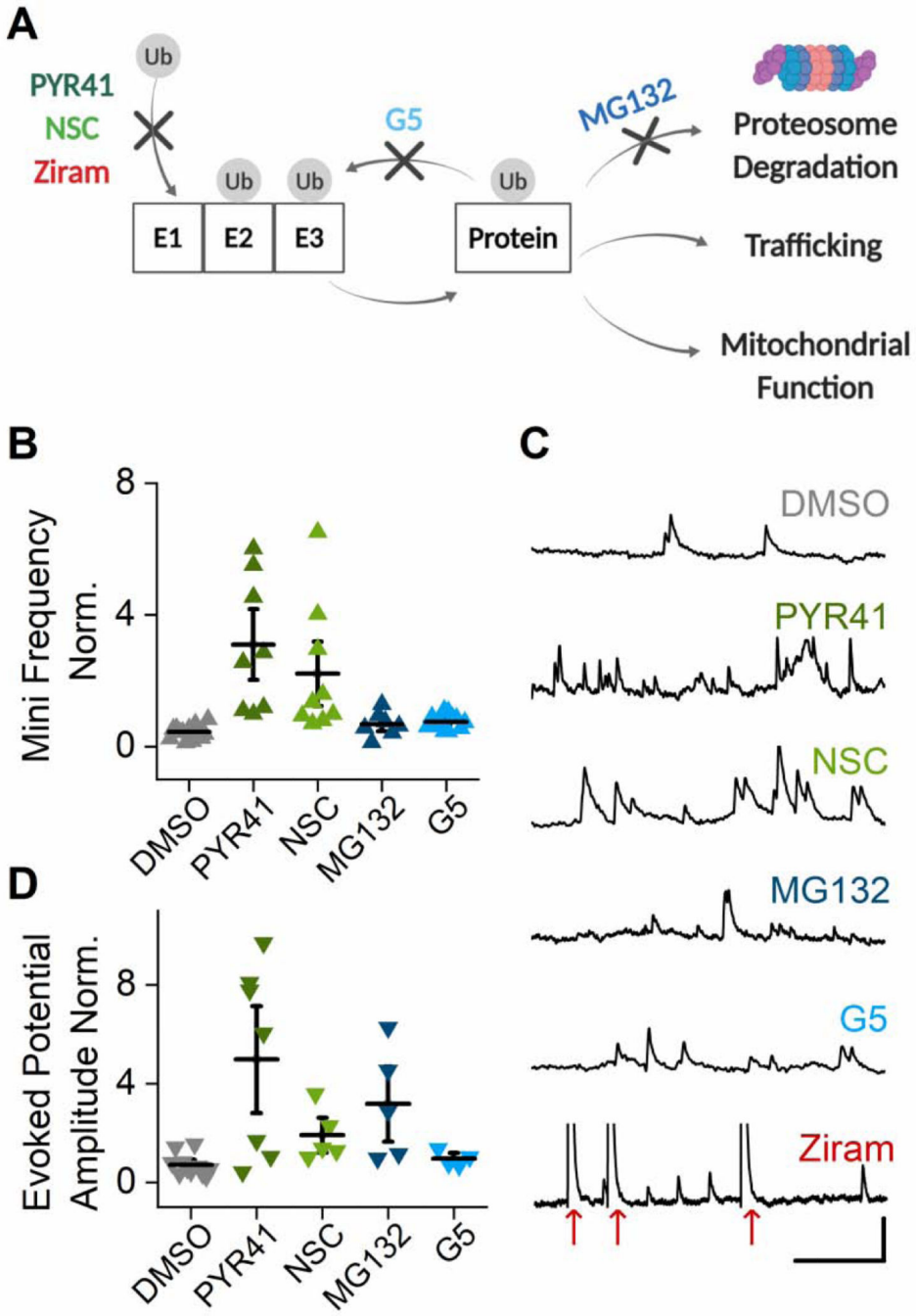

Figure 8. Disruption of the Ubiquitin Signaling System enhances vesicle release probability, but not excitability.

A. Simplified diagram of the Ubiquitination Signaling System (USS) with sites of pharmacological inhibition indicated: E1 activating enzyme (PYR41, NSC, ziram), deubiquitinating enzyme (G5) and the proteasome (MG132). **B.** Normalized mini frequency in control (n=13), PYR41 (5 μM; n=8), NSC (20 μM; n=9), G5 (10 μM; n=12), and MG132 (10 μM; n=7) (mean ± SEM). **C.** Sample traces of minis following addition of control, PYR41, NSC, MG132, G5, and ziram. Note that unlike ziram, PYR41, NSC, MG132, and

G5 do not induce EJPs (indicated by red arrows). Scale is 500 ms and 1 mV. **D.** Normalized evoked potential amplitude following the addition of control (n=11), PYR41 (n=7), NSC (n=7), GS (n=4), and MG132 (n=5).

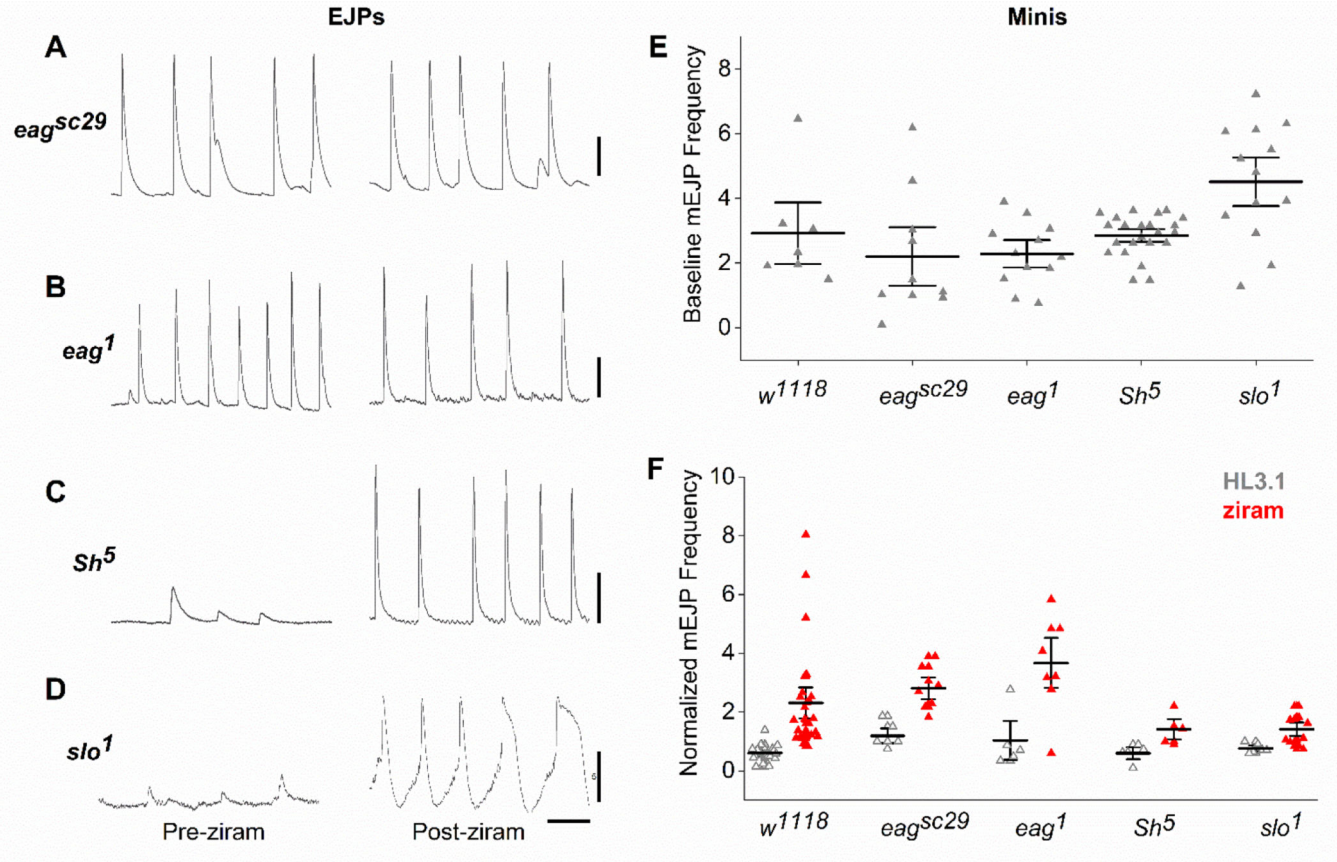

Figure 9. Ether-a-go-go potassium channel mutants phenocopy and occlude ziram-induced excitability, but not the ziram-induced changes in vesicle release probability.

A-D. Representative traces of spontaneous EJPs in the *eag*^{sc29}, *eag*^{1}, *Sh*^{5}, and *slo*^{1} mutants in control (*left*) and after perfusion of 10 μM ziram (*right*, *eag*^{sc29} n=10, *eag*^{1} n=6, *Sh*^{5} n=5, and *slo*^{1} n=8). Scale is 200 ms and 5 mV. Ziram does not enhance EJP frequency in *eag* mutants. Ziram both increases mini frequency and elicits EJPs in *Shaker* and *slowpoke* mutants. **E.** Baseline mini frequencies during a five-minute recording period in wildtype and K channel mutants. **F.** Mini frequencies after perfusion of a second solution (control: grey open triangles; 10 μM ziram: red triangles). 1 μM TTX added to experiments using *eag* mutant animals. Mini frequencies were measured in wildtype and the following potassium channel mutants: *eag*^{sc29} (control n=5; ziram n=10), *eag*^{1} (control n=6; ziram n=6), *Sh*^{5} (control n=7; ziram n=5), *Sh*^{KS133} (control n=7; ziram, n=7; data not shown), and *slo*^{1} (control n=5; ziram n=8). Note that ziram increases mini frequency independent of genotype.

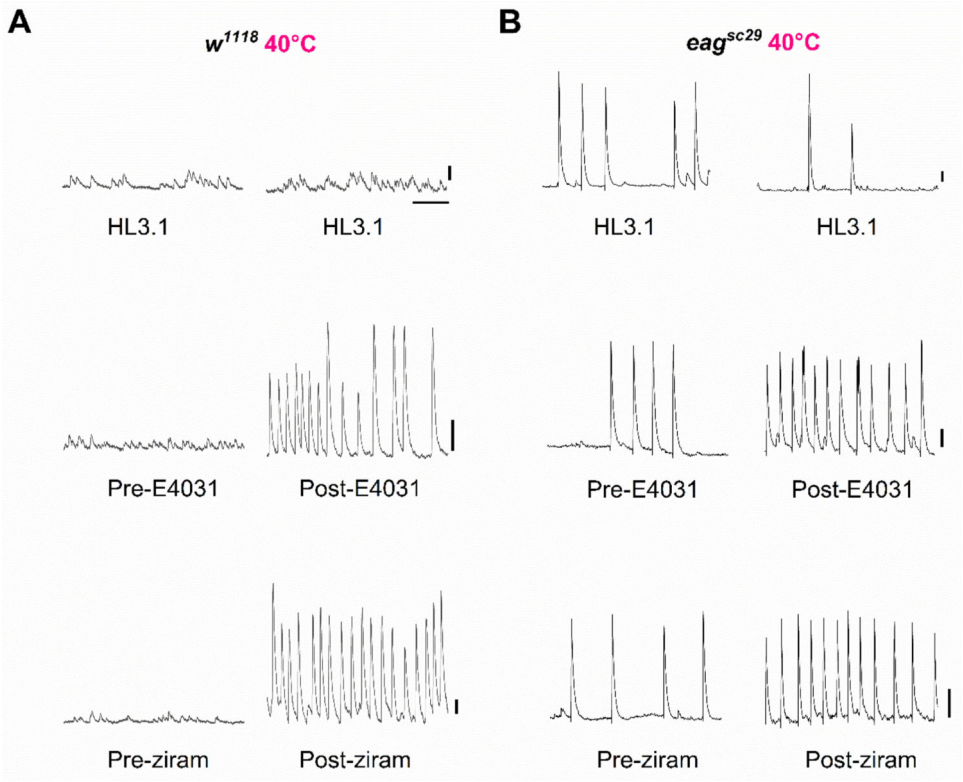

Figure 10. Ziram and E4031 enhance excitability at elevated temperature.

A. Representative traces of minis in wildtype (w^{1118}) animals at baseline (*left*) and with control, 100 μM E4031, or 10 μM ziram (*right*) recorded at 40°C (control n=7, E4031 n=8; ziram n=9). Scale bar is 200 ms and 5 mV. **B.** Representative traces of EJP Frequency in eag^{sc29} null mutants at baseline (*left*) and with control, 100 μM E4031, or 10 μM ziram solution recorded at 40°C (control n=19, E4031 n=8, ziram n=12). Scale bar is 200 ms and 5 mV.

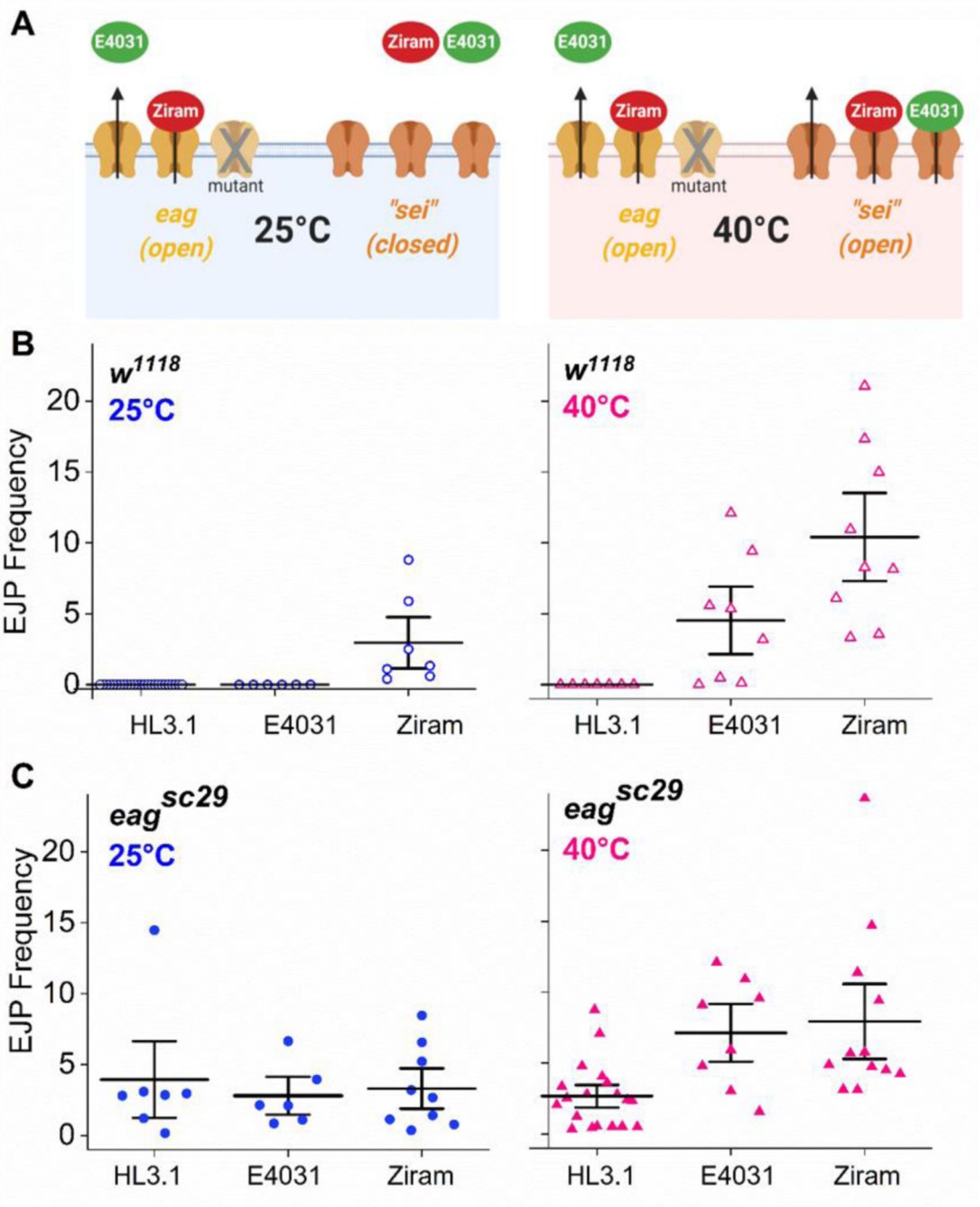

Figure 11. At 40°C ziram blocks both eag and "sei" potassium channels.

A. Proposed mechanism: at 25°C, ziram inhibits the eag K channel to increase excitability and *eag* null mutants also show enhanced excitability. E4031, a hERG channel blocker, has no effect since most sei channels are closed (*left).* At 40°C, sei channels are thought to be active. Both ziram and E4031 inhibit "sei" to drive excitability in wildtype and *eag* mutants. Ziram increases excitability by blocking both "sei" and eag (*right).* **B.** EJP frequency in wildtype at 25°C (*left*) in control (n=25), E4031 (n=6) and ziram (n=7) and in experiments performed at 40°C (*right;* control, n=7, E4031, n=8; ziram, n=9). **C**. EJP

frequency in *eag*^{sc29} null mutants at 25°C (*left)* in control (n=7 E4031 (n=6), and ziram (n=9) and in experiments performed at 40°C (*right;* control, n=19; E4031 n=8; ziram n=12). Since the target of the E4031 is not unequivocally sei and could potentially be another temperature sensitive channel, the name is depicted in quotation marks ("sei," see main text for discussion).